nature methods

ARTICLES

https://doi.org/10.1038/s41592-020-0961-2

EthoLoop: automated closed-loop neuroethology in naturalistic environments

Ali Nourizonoz[1], Robert Zimmermann[1], Chun Lum Andy Ho[1], Sebastien Pellat[1], Yannick Ormen[1], Clément Prévost-Solié[1], Gilles Reymond[1], Fabien Pifferi[2], Fabienne Aujard[2], Anthony Herrel[2] and Daniel Huber[1]✉

Accurate tracking and analysis of animal behavior is crucial for modern systems neuroscience. However, following freely moving animals in naturalistic, three-dimensional (3D) or nocturnal environments remains a major challenge. Here, we present EthoLoop, a framework for studying the neuroethology of freely roaming animals. Combining real-time optical tracking and behavioral analysis with remote-controlled stimulus-reward boxes, this system allows direct interactions with animals in their habitat. EthoLoop continuously provides close-up views of the tracked individuals and thus allows high-resolution behavioral analysis using deep-learning methods. The behaviors detected on the fly can be automatically reinforced either by classical conditioning or by optogenetic stimulation via wirelessly controlled portable devices. Finally, by combining 3D tracking with wireless neurophysiology we demonstrate the existence of place-cell-like activity in the hippocampus of freely moving primates. Taken together, we show that the EthoLoop framework enables interactive, well-controlled and reproducible neuroethological studies in large-field naturalistic settings.

A precise quantification of behavior is essential for understanding brain function. Neuroscientists and ethologists have studied animal behavior for decades seeking to identify the underlying neural circuits[1,2]. The quest for linking neuronal activity to specific behaviors in a laboratory setting imposes several constraints on experimental frameworks[3]. Besides the obvious need for tractable variables, the studied behavior should retain most ethologically relevant sensory, motor and cognitive components, while remaining reproducible. The environmental setting in which the animal moves should also be flexible enough to allow probing for multiple parameters involved in the studied behavior. Finally, simultaneous recordings or manipulations of neuronal activity is essential.

One strategy is to partially or fully immobilize the animals in a virtual reality environment[4]. This approach facilitates detailed observation of behavior and allows for accurate closed-loop stimulus control. It can also provide convenient and stable access to the brain for optical[5,6] or electrophysiological recordings[7]. However, important drawbacks exist[8]. In most instances, natural motor output and the related sensory feedback are substantially disrupted, possibly inhibiting normal spatial processing[9] (although see refs. [10,11]). Furthermore, virtual reality is often limited to a single sensory modality, such as vision[4–6,12], somatosensation[13] or olfaction[14]. Finally, studying typical primate motor patterns such as climbing or jumping and probing behaviors such as social interactions involving multiple animals is more challenging in virtual reality.

An alternative approach is to retain the animal's full sensorimotor experience by studying its behavior while the animal is freely moving in naturalistic environments. This, however, poses challenges regarding behavioral control and quantification. It necessitates knowing where the animal is and what it does, as well as tracking the identity of multiple subjects. Systems for tracking in naturalistic environments have been developed for several animal species, including insects[15–19], rodents[20–22], primates[23,24] or flying bats[25,26]. Multiple subject identification can be achieved based on the recognition of coat color[27], wearable colored markers[23,28], electronic markers[29], Kalman and nearest neighbor filters[17] or deep learning[19,30]. Finally, immersive visual virtual reality for unrestrained animals has also been developed[11,31,32]. However, by projecting a single viewpoint into the arena, these systems are currently restricted to the use with single animals, and provide only nonbinocular views. In general, most tracking systems are limited by small and relatively empty laboratory environments, and require bright and even illumination (although see refs. [23–25]) to extract position and behavior or to provide feedback. Studying animals in more naturalistic environments with noisy or changing backgrounds and poorly lit conditions (for example, in arboreal and nocturnal settings), poses serious challenges to most existing tracking systems.

Finally, interacting with freely roaming and fast-moving animals in a closed-loop manner for behavioral conditioning would require a tracking framework to be extremely fast, robust and to provide sufficient high-resolution information about the tracked animal. However, most current systems for freely moving animals are still designed for offline behavioral analysis (although see refs. [11,19,31–34]) and thus cannot react to behavioral elements in the order of tens of milliseconds. Taken together, there is currently a need for an integrated framework able to carry out the next generation of reproducible neuroethological experiments with freely moving animals in more naturalistic settings.

Results

Implementation of the EthoLoop tracking system. To follow the behavior of freely roaming nocturnal animals, such as mice (*Mus musculus*) or mouse lemurs (*Microcebus murinus*, a small arboreal primate), in naturalistic 3D environments, we developed an ultra-fast, multi-camera closed-loop tracking system capable

[1]University of Geneva, Department of Basic Neurosciences, Geneva, Switzerland. [2]Musée National d'Histoire Naturelle, Adaptive Mechanisms and Evolution, UMR7179—CNRS, Paris, France. ✉e-mail: daniel.huber@unige.ch

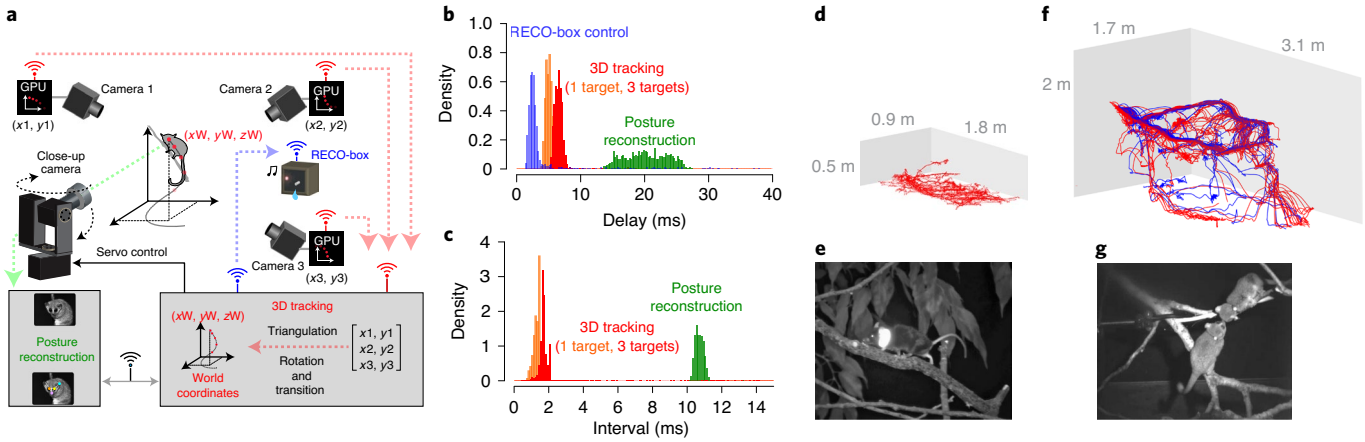

Fig. 1 | The EthoLoop behavioral tracking system. a, Schematic depiction and spatial arrangement of the different EthoLoop elements. Multiple infrared cameras (cameras 1–3) with dedicated GPUs process images from different viewing angles. The identity and positions of the detected markers are wirelessly transmitted to a central host computer for 3D reconstruction (triangulation, followed by rotation and transition into real-world 3D coordinates). The 3D coordinates are forwarded to control the position and focus of a gimbal-mounted close-up camera. The images from the close-up system are either saved for offline analysis or processed on-the-fly to trigger remote-controlled reward boxes (RECO box). RECO boxes are connected wirelessly and can provide auditory or visual stimuli or liquid rewards. **b**, Latencies for the communication with the RECO box (blue), reconstructing 3D position (1 and 3 targets, orange and red), and the real-time posture analysis (green). **c**, Intervals for consecutive reconstitutions (1 and 3 targets, orange and red) and time for the postural analysis (green) of two subsequent frames. **d**, 3D trajectory of a mouse tracked in a naturalistic environment (red line, 60 min, Supplementary Video 1), in an arena covered with wooden branches (representative example of 26 experiments). The tracking was carried out in the dark and based on a passive retro-reflective marker fixed around the neck. **e**, Still image from the infrared close-up camera following the position of the tracked mouse in **d**. **f**, 30 min of 3D trajectories of two mouse lemurs (red, blue) tracked in an arena filled with tree branches (representative example of 20 experiments). **g**, Infrared close-up image of the two tracked mouse lemurs (from **f**).

of providing simultaneous close-up views and analyses of the ethology of tracked individuals (Fig. 1). We hence termed the system EthoLoop.

Multiple high-speed infrared cameras are installed above a tracking arena, providing views of the freely moving animals from different angles (Fig. 1a). The images from each camera are processed separately to extract the two-dimensional (2D) positions of each animal. The identification and tracking of individuals in the dark is either achieved using retro-reflective passive markers (Fig. 1d and Supplementary Video 1) or, when multiple individuals have to be tracked simultaneously, by spectrally separating the hue of miniature battery-powered infrared light emitting diodes (LEDs) with different wavelengths (Fig. 1f, Supplementary Fig. 1 and Supplementary Video 2). To increase the speed and decrease the processing time, the spatial localization and spectral separation of each camera view is carried out on stand-alone graphical processing units (GPUs) (Fig. 1a). The position of each animal is then transformed into real-world 3D coordinates by geometric triangulation[17,23] from the different camera views (Fig. 1a). We achieved maximal tracking at rates ranging from 785 to 580 Hz (for 1–3 targets, 1 ms exposure time, Fig. 1c), with delays below 8 ms for up to three targets (Fig. 1b and Supplementary Fig. 2). The ideal number of cameras (minimum 2) depends on the complexity of the obstructing structures in the environment. Adding more cameras can also improve the tracking accuracy in larger arenas, if they reduce the minimal distance to the target. Thus, by combining off-the-shelf hardware and open source code, this system can be adapted to spatial scales of 1 m^3 (Fig. 1a and Supplementary Video 1), 10 m^3 (Fig. 1f and Supplementary Videos 2 and 3) and up to 100 m^3 (Supplementary Fig. 3 and Supplementary Video 4). Tracking multiple animals in such large arenas while preserving their respective identity allows detailed study of their social interactions (Supplementary Fig. 4). Finally, to facilitate the installation of additional cameras in large-scale and challenging conditions (trees, branches), all cameras and GPUs can be battery-powered and communicate via wireless network protocols, thus removing the need for external wiring and facilitating their placement in strategic locations.

Although the GPU-based 3D tracking allows determining the animal's position with high temporal resolution (Fig. 1b,c) and precision (Supplementary Fig. 1i), it does not provide any information about the actual behavior carried out at that location. Inspired by the pioneering work on freely flying and walking insects[15,17], we therefore added a gimbal-mounted, close-up video camera to the EthoLoop system, providing a focused and magnified view continuously centered on the tracked individual (Fig. 1e,g and Supplementary Video 3). This way, the behavior of a tracked animal can be analyzed in detail, independent of the actual size of the tracked volume in which it navigates. Since jumping primates can reach speeds up to 2 $m\,s^{-1}$ (Supplementary Video 3), the focusing mechanism of the close-up system was driven by a liquid lens capable of changing focus within milliseconds. Although we only used a single close-up view for our experiments, the position of one or multiple animals can be forwarded to multiple close-up systems in parallel. To ensure sufficient illumination of the tracked subject in dark large-scale environments, we mounted an infrared light source in parallel to the camera path (Supplementary Video 4) or on a separate gimbal system. This allowed a targeted and economical illumination independently of any ambient light. In summary, the EthoLoop system combines fast and accurate tracking of animal position even in large, arboreal or nocturnal settings with high-resolution close-up views of their behavior.

Observation and manipulation of natural foraging behavior using remote-controlled reward sources. Out of all animal behaviors, foraging is most likely one of the most universal activities[35,36]. It was probably a prominent driver behind main evolutionary specializations of sensory, motor and cognitive capacities in primates and other clades[37]. To study naturalistic foraging in laboratory settings, the distribution of food sources, as well as sensory cues signaling their availability would ideally be controlled by the experimenter

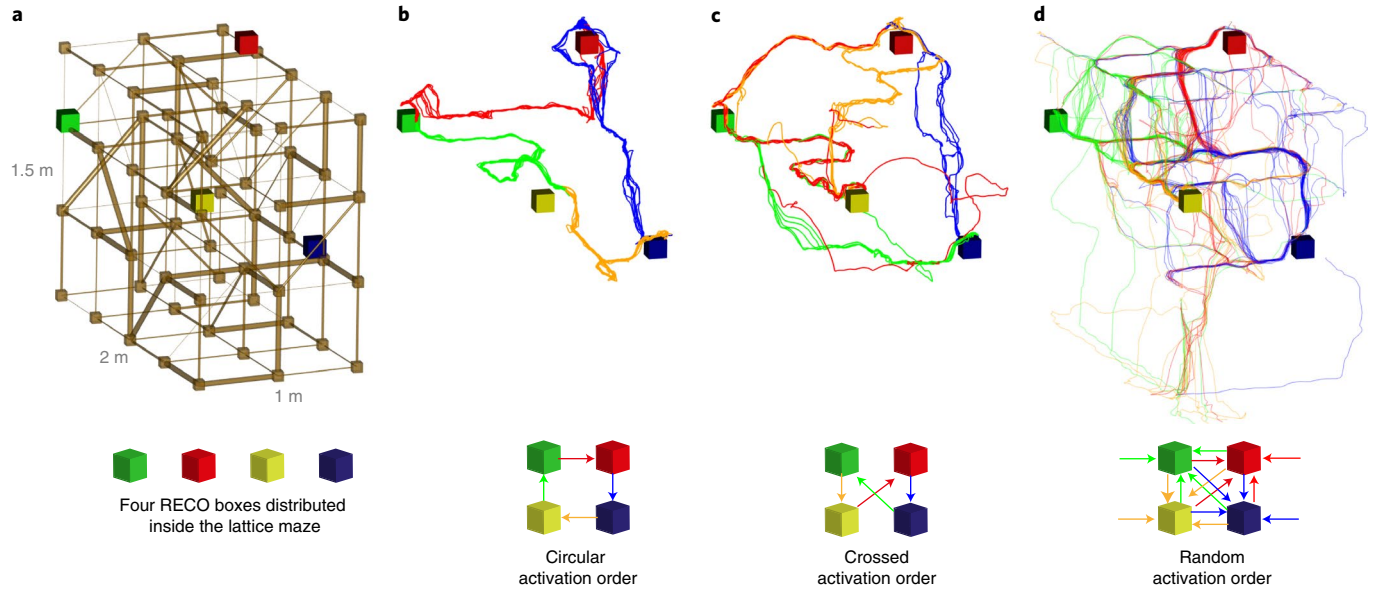

Fig. 2 | Foraging of a mouse lemur in a 3D lattice maze. a, Four RECO boxes (colored cubes) spatially distributed at different locations of a lattice maze (0.5 m branch length). RECO boxes are shown in different colors and are activated with different sequences. Reward availability was indicated by a 9 kHz tone. The actual reward delivery was made conditional on the animal's arrival at the feeder within 10 s. **b**,**c**, 10 min of 3D trajectory of the mouse lemur where the RECO boxes are activated in a circular (**b**) or crossed order (**c**). The trajectory color indicates the currently activated RECO box (representative trajectories of eight experiments). **d**, 3D trajectory of a mouse lemur when activation order was random and conditional on the actual position of the animal in the arena (representative trajectory of four experiments).

in real time, taking into account the animal's actual position and behavior. This way, specific situations could be created in a reproducible manner. We therefore integrated small, remote-controlled and interactive reward boxes (RECO box) into the EthoLoop framework. The RECO boxes are able to play sensory cues (auditory or visual) and provide calibrated amounts of liquid rewards (Fig. 1a and Supplementary Fig. 5a,b). Multiple of these battery-powered boxes can be distributed in the environment to mimic the availability and cues associated with natural resources.

To illustrate the range of basic behavioral patterns in freely roaming mouse lemurs, we positioned multiple RECO boxes in the behavioral arena (Fig. 2a and Extended Data Fig. 1a). To cover the volumetric space more evenly and make the experiments more reproducible, we also replaced the naturalistic branches with a parameterizable artificial lattice maze[38,39]. The availability of a liquid reward at a given location was indicated by an auditory cue (9 kHz tone, 1 s intermittent at 0.5 Hz). To mimic a variable degree of predictability of the next food location, we first activated the different boxes sequentially in a fixed order (Fig. 2b,c, Supplementary Video 5 and Extended Data Fig. 1b,c). This type of activation triggered highly stereotypical and most likely memory-guided paths. On the other hand, the random activation of a RECO box (triggered by the specific spatial location of the animal, Fig. 2d) established a situation where the animal could not predict the next reward location, and hence resulted in more variable behavioral patterns (Fig. 2d). The location-triggered random activation allowed us to have the mouse lemurs cover a large part of the 3D lattice maze (Fig. 2b,c). These data illustrate how combining real-time tracking with remotely controlled elements can rapidly shape specific behaviors and force the animals to adopt different foraging strategies.

Other, more global environmental parameters such as illumination also affect behavior in a given environment[36]. To highlight how our system can detect behavioral signs related to such global parameter changes, we reduced the illumination levels from dim (<1 lux, Extended Data Fig. 1d) to complete darkness (Extended Data Fig. 1e and Supplementary Video 6). This triggered a profound change in the movement parameters including a reduction in the number of jumps (Extended Data Fig. 1f), or the locomotor speed distribution (Extended Data Fig. 1g and Supplementary Video 6).

Taken together, the combination of the EthoLoop tracking system with interactive agents, such as RECO boxes, or changes of global parameters, such as illumination, is ideally suited for exploring different aspects of ethologically relevant parameters within naturalistic settings.

Fully automated conditioning of behavior in naturalistic settings. To explore the possibility of using the EthoLoop system to reinforce specific behaviors by operant conditioning[40], we combined the principle of clicker training by human experts[41,42] with real-time and automated behavioral analysis. An auditory stimulus (9 kHz tone) followed by a small liquid reward from one of the RECO boxes was triggered on an automated detection of a specific behavior. To test the effectiveness of such automated conditioning procedures, we first conditioned mice to enter an arbitrarily chosen location in a naturalistic environment designed with tree branches (Fig. 3a and Extended Data Figs. 2 and 3). On detecting an entry into a defined location, the tracking system triggered a sound from a single RECO box and a reward was available for the subsequent 10 s in the center of the arena. Mice learned the task (Fig. 3b–d and Extended Data Fig. 2b), and the number of entries into the conditioned area increased compared to the initial rate (Fig. 3d and Extended Data Fig. 2b–f). Similarly, we were able to condition a mouse lemur to climb repeatedly to an experimenter-defined position within the 3D lattice maze (Fig. 3e and Extended Data Fig. 4a). The number of entries increased over a 30 min session (Fig. 3f–h and Extended Data Fig. 4b,c).

Inspired by more sophisticated behavioral conditioning experiments carried out by professional animal trainers with pets or zoo animals[41,42], we further sought to use the real-time close-up video stream to automatically detect specific postures[43] and reinforce them using the RECO boxes. As a proof of principle, we chose to reinforce rearing behavior, which is observed spontaneously in

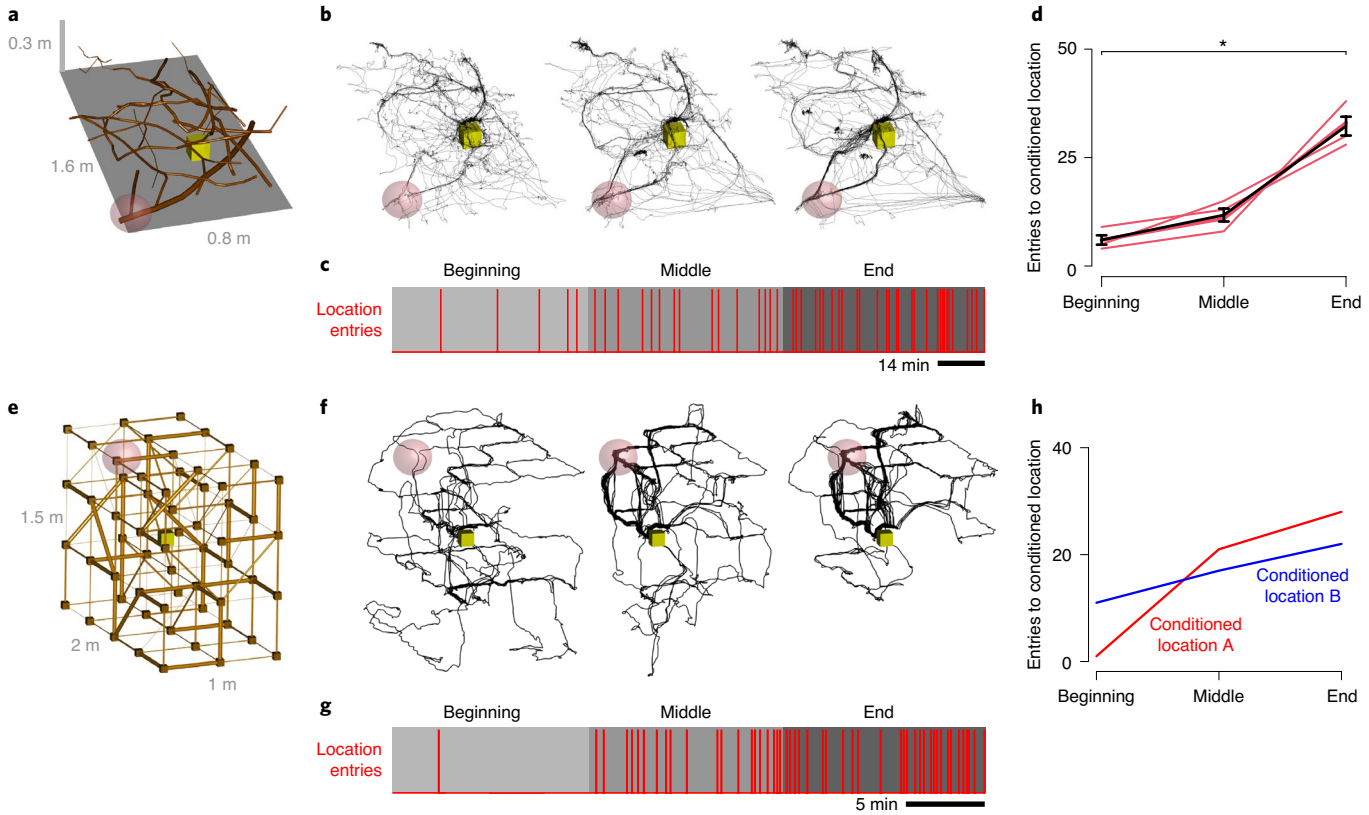

Fig. 3 | Fully automated place conditioning in 3D environments. a, An arena for freely moving mice covered with tree branches containing a single RECO box. Mice were trained to visit an unmarked location on a branch (red sphere). The reinforced location was changed daily. **b**, Example of a 3D trajectory of a mouse in the beginning, middle and end of a behavioral session (all other trajectories in Extended Data Fig. 2). **c**, Entries to the conditioned place across a behavioral session of **b**. **d**, Number of entries to the conditioned place. Mice entered the conditioned place more frequently ($N = 4$ mice, third day, one-way repeated measure ANOVA, $F(2,6) = 46.867$, main effect $P = 0.0002$, pairwise two-sample t-test, Bonferroni correction for multiple comparison, beginning versus end, $^*P = 0.01$). Bars represent standard error of mean. **e**, Place conditioning of mouse lemurs in a 3D lattice maze. The red sphere indicates the conditioned location. **f**, Trajectories of a mouse lemur in the beginning, middle and end of a behavioral session (all other trajectories in Extended Data Fig. 4). **g**, Number of entries to the conditioned place across the behavioral session in **f**. **h**, The number of entries increases for different conditioned places. The two colors represent the conditioning at two different locations for the same mouse lemur (Extended Data Fig. 4).

both mice and mouse lemurs (Fig. 4). To detect rearing, we first trained a deep-learning network (DeepLabCut[44]) to track different body parts in a set of hand-annotated close-up videos (Fig. 4a). In a second step, we adapted DeepLabCut to classify the streamed images and localize the position of the different body parts in real time in the stream of close-up images (Fig. 4a). Using this procedure, we were able to identify body parts at an average rate of 93 Hz (Fig. 1c, green histogram) using a standard commercial computer graphics card. In a third step, the rearing behavior was detected using a set of geometrical rules, taking into account the relative spatial position of body parts. Reinforcing automatically detected rearing with a click (9 kHz), followed by a reward from a nearby RECO box (Fig. 4a), mouse lemurs rapidly increased the number of rearings (red arrows in Fig. 4g,h,i and Supplementary Video 7). In parallel, we also conditioned mice to rear on top of a branch in a naturalistic environment (Fig. 4b and Extended Data Fig. 5) and at a specific location in an open-field arena (Extended Data Fig. 6). Mice increased the number of rearings within the session (Fig. 4c–e and Supplementary Video 8). These experiments illustrate how real-time and automated behavioral classification by the EthoLoop system can be efficiently used to shape or reinforce specific actions in situations that would have been very challenging to do for any trained human observer (due to fast-moving subjects, poor illumination, large arenas or partial occlusions).

Operant conditioning by optogenetic stimulation of reward circuits. Using behavior-triggered operant conditioning with actual cues and rewards can become problematic when multiple subjects are present in the vicinity, since the reinforcement should target only one individual. Individualized conditioning can be achieved by optogenetic tools; for example, by the selective activation of dopamine (DA) neurons in the ventral tegmental area (VTA)[45]. We tested whether behaviors detected by the EthoLoop system can also be reinforced by real-time optogenetic stimulation of VTA DA neurons in mice (Fig. 5).

We first conditioned mice to enter a specific location in the arena by optogenetically activating VTA DA neurons either wirelessly through a portable, battery-powered stimulator (Supplementary Fig. 6) in naturalistic environments (Fig. 5b), or tethered via an optical fiber connected to a blue laser in open-field environments. Within single sessions, we successfully conditioned mice to enter a defined place more often (Fig. 5e and Extended Data Fig. 7).

In a second set of experiments, VTA DA neurons were activated on the detection of a predefined behavioral syllable[43]. As before (Fig. 4), we chose to reinforce rearing on the hind limbs (Fig. 5a). On reinforcement with optogenetic VTA stimulation, mice started rearing more within the specified area (Fig. 5g,i, Extended Data Fig. 8 and Supplementary Video 9). These experiments show that the EthoLoop system is well suited to provide precisely timed and

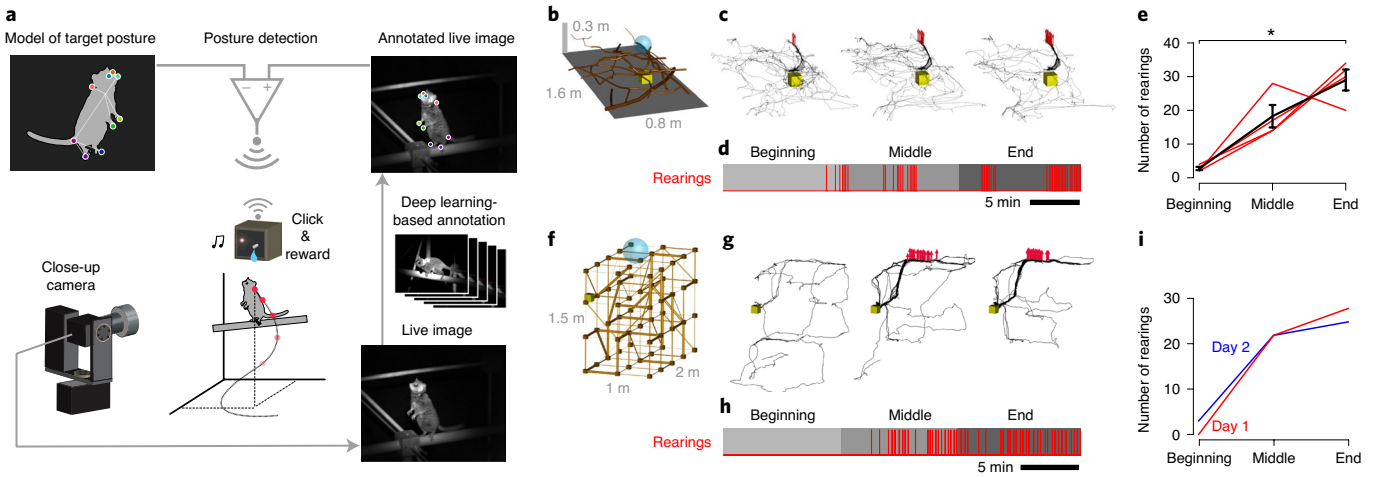

Fig. 4 | Operant conditioning of automatically detected behavior. a, Schematic representation of the information flow. While the close-up camera provides high-resolution live images of the tracked animal, the body parts are classified in real time by the weights of a pretrained deep-learning network. A match of the annotated live image with a geometric model of the posture to be reinforced, will trigger a sound, followed by a reward in the RECO box. **b**, The naturalistic environment designed with tree branches for mice with a RECO box (yellow cube) and an experimenter-defined area where rearing was conditioned (blue sphere). **c**, Trajectory of a mouse during a conditioning session where the number of rearings increased (all other trajectories in Extended Data Fig. 5). **d**, Rearings detected across the session in **c**. **e**, Summary data of the number of rearings detected across all sessions. The number of rearings increased within a behavioral session ($N=4$ mice, one-way repeated measure ANOVA, $F(2,6)=16.618$, main effect $P=0.004$, pairwise two-sample t-test, Bonferroni adjustment for multiple comparison, $^*P=0.009$). Bars represent standard error of mean. **f**, The lattice maze for mouse lemurs with a RECO box (yellow cube) and an experimenter-defined area where rearing was conditioned (blue sphere). **g**, Three-dimensional trajectory of a mouse lemur during a conditioning session (representative trajectory of two experiments). The red arrows indicate rearing. **h**, The number of rearings detected across the session in **g**. **i**, Number of detected rearings across two sessions (days 1 and 2) with the same mouse lemur.

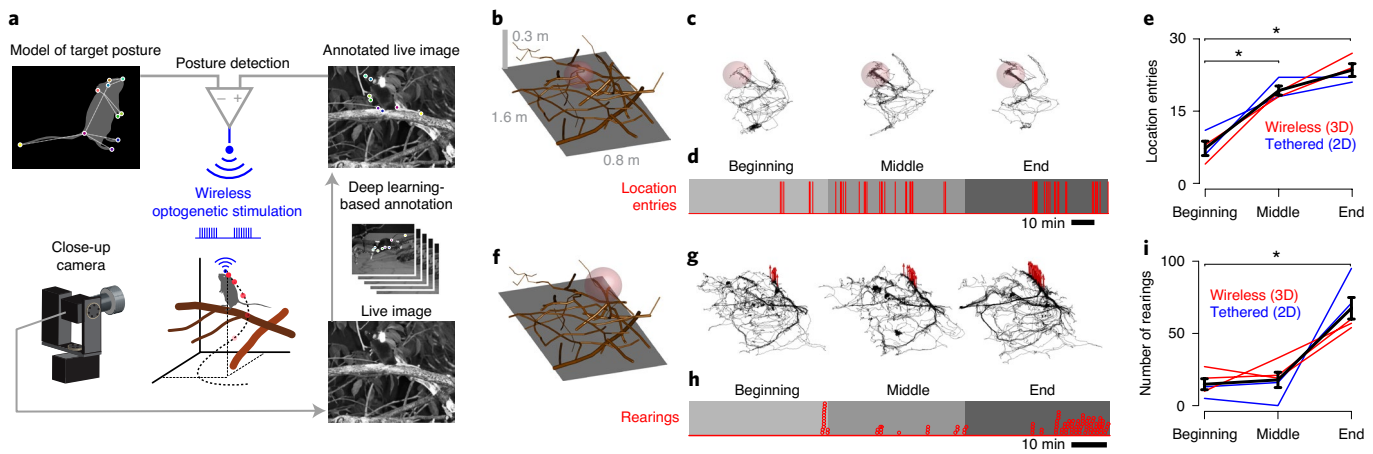

Fig. 5 | Reinforcing automatically detected behaviors using optogenetic VTA stimulation. a, Schematic representation of the information flow during conditioning by optogenetic activation of VTA DA neurons. The steps are identical to Fig. 5, except that the detection of a behavioral event wirelessly triggered the optogenetic stimulation of VTA DA neurons through a portable, battery-powered stimulator (Supplementary Fig. 6). **b**, Naturalistic environment covered with tree branches for freely moving mice. The red sphere indicates the conditioned location. **c**, Trajectory of a mouse in the beginning, middle and end of a conditioning session with wireless optogenetic stimulation (all other trajectories in Extended Data Fig. 7). **d**, Occurrence of entries to the conditioned location across a session (from **c**). **e**, Summary data for the second day of place conditioning using wireless optogenetic VTA stimulation in naturalistic (3D, red) and tethered stimulation in an open-field arena (blue). The number of entries to the conditioned place increased within a session ($N=4$ mice, combined 3D and open-field arena, one-way repeated measure ANOVA, $F(2,6)=29.137$, main effects $P=0.0008$, pairwise two-sample t-test, Bonferroni correction for multiple comparison, beginning versus end, $^*P=0.023$, beginning versus middle, $^*P=0.026$). **f**, Same arena as in **b** with the red sphere indicating the predefined location where rearing triggered VTA DA stimulation. **g**, Trajectory of a mouse during a session with optogenetic reinforcement of an automatically detected posture (rearing, red arrows; all other trajectories in Extended Data Fig. 8). **h**, Rearings detected across the session in **g** shown in red dots. **i**, Number of rearings detected at the beginning, middle and end of the behavioral session with wireless (red) and tethered (blue) optogenetic stimulations. The number of rearings increased within single sessions ($N=5$ mice, one-way repeated measure ANOVA, $F(2,8)=17.73$, main effect $P=0.001$, pairwise two-sample t-test, Bonferroni correction for multiple comparison, $^*P=0.023$). Bars represent standard error of mean in **e** and **i**.

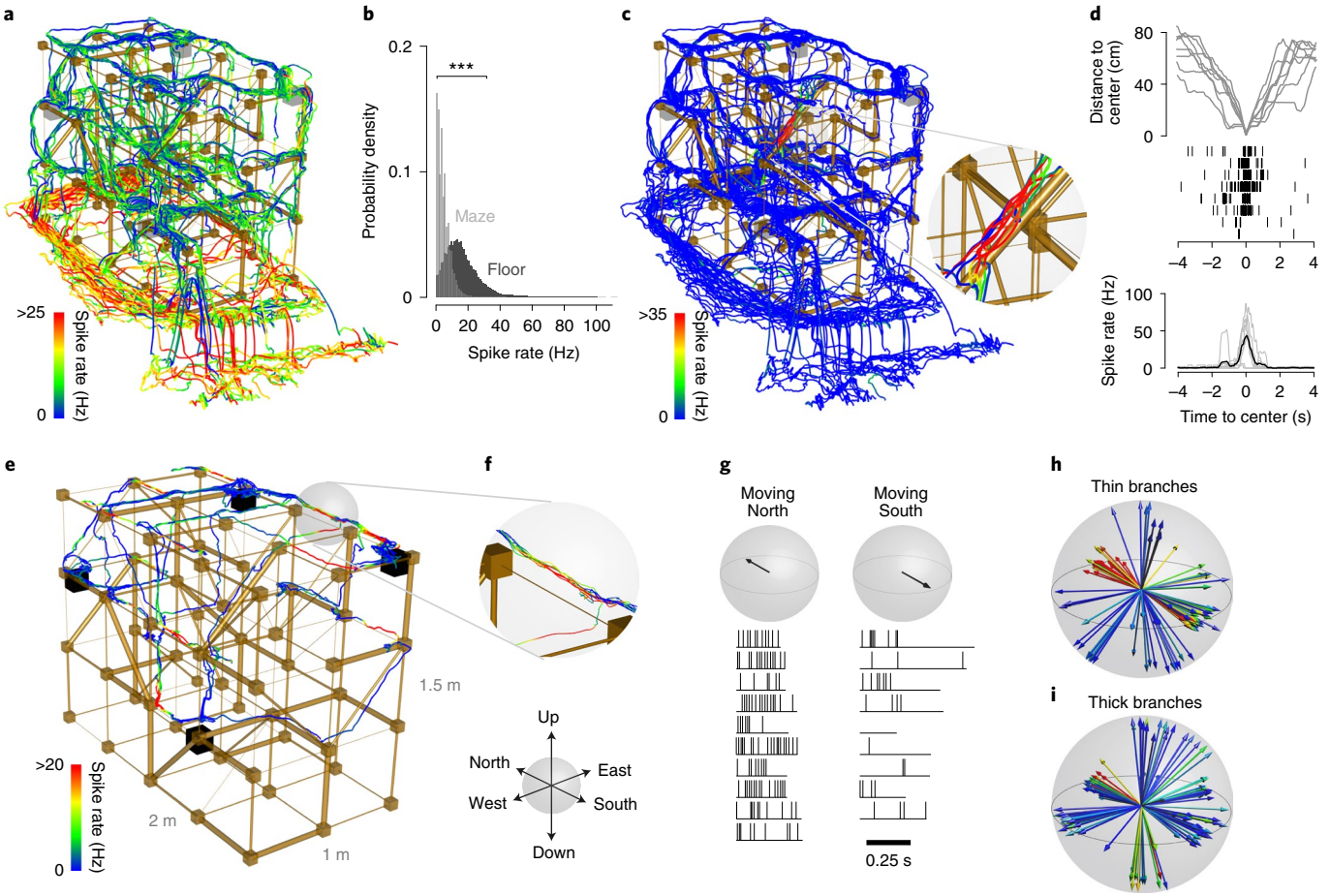

Fig. 6 | Wireless recordings of neuronal activity in dorsal CA1 during navigation in a 3D lattice maze. a, A neuron in mouse lemur CA1 during foraging in a lattice maze showing increased spike rate when on the floor. **b**, The neuronal activity (over segments of 13 cm) on the floor compared to the activity in the rest of the lattice maze (***$P < 2.2 \times 10^{-16}$, two-sample Kolmogorov–Smirnov test). **c**, Spike rates for a CA1 neuron showing increased activity preferentially on a single branch location (same recording session as in **a**. **d**, Distance of the animal to the location with highest average activity (top), action potentials of the recorded neuron (middle) and spike rate of the recorded neuron during individual passages (gray) and their average (black), in relation to the time to reach the center (highest average activity). **e**,**f**, Spike rates of a CA1 neuron showing increased activity on multiple locations in the maze. **g**–**i**, Additional analysis revealed that the neuronal activity was specific to one specific spatial direction (**g**) (north, neuronal data from the location in the gray sphere in **e** and higher when moving north on thin (**h**) compared to thick branches (**i**). The arrows in the sphere indicate the movement directions (13 cm segments), while the color indicates the level of activity.

behaviorally triggered optogenetic stimuli to freely moving animals in a fully automated manner and thus shape specific behavioral elements within single behavioral sessions.

Combining 3D tracking with wireless neuronal recordings. The ultimate goal of many neuroethological studies is to link a specific behavior to its underlying neuronal activity. To illustrate the feasibility of simultaneous neuronal recordings in combination with actively controlled foraging (Fig. 2), we set up a miniature wireless electrophysiological recording system for freely moving mouse lemurs. We recorded neurons in the dorsal CA1 of hippocampus (Supplementary Fig. 7), a brain area related to various aspects of spatial navigation[46–48].

By synchronizing the recorded activity with the 3D position of the mouse lemur (Fig. 6) we found neurons that were responsive to a large region (floor, Fig. 6a,b) or a specific location (single branch, Fig. 6c,d and Extended Data Fig. 9) of the lattice maze, or mainly when moving in one direction on branches with a given diameter (Fig. 6e–i and Extended Data Fig. 10). The EthoLoop system allowed us to induce the specific foraging patterns and thus ensure that the animals either cover large parts of the lattice maze (Fig. 6a,c) or create multiple reproducible paths across a given location (Fig. 6e). These recordings are to our knowledge among the first examples of 3D place cell-like activity recorded in freely roaming primates and illustrate the vast potential for future experiments when combining the EthoLoop system with wireless electrophysiology.

Discussion

EthoLoop is a video tracking framework that allows following animal behavior in naturalistic environments. More importantly, it can actively shape behaviors via closed-loop interactions. Such active interaction with the tracked subjects opens possibilities for many types of experiment ranging from automated reinforcement of innate sequences to the learning of complex cognitive tasks.

Furthermore, its scalability as well as its wireless connectivity to battery-powered optogenetic stimulation and electrophysiological recording devices make it a powerful tool for characterizing complex behaviors in large-scale and naturalistic settings. The possibility of using batteries also as a power source for cameras and RECO boxes furthermore opens the door to study the behavior of wild animals in their natural habitats. Adding more tracking and close-up cameras will be necessary, however, if foliage or branches

are too obstructive or if the behavior of multiple animals needs to be characterized simultaneously at high resolution.

We have shown that synchronized optogenetic manipulations and electrophysiological recordings during free navigation are, in principle, feasible. Similar to the pioneering work with freely flying bats[25,26,49] we have chosen data loggers as recording devices. For future closed-loop experiments involving triggering events by neuronal activity, actively transmitting recording systems will be necessary.

Our experiments illustrate that the EthoLoop system is ideally suited to studying behaviors such as foraging[35]. Foraging provides a unique setting where not only the limits of multi-sensory integration, sensory-guided motor control, high level cognition or 3D spatial navigation[25,26,39,49] can be probed in a reproducible manner, but it can also become a powerful tool for dissecting neuronal dynamics underlying decision making and economic choice[35].

The overall principles of the EthoLoop framework (close-up view, online classification, interaction with RECO boxes) are also applicable to other real-time tracking systems[11,15–18,23,29] and might thus be combined with already existing hardware (as long as the relative position can be updated fast enough). Finally, the recent emergence of markerless methods for tracking multiple subjects[19] or for behavioral analysis going beyond basic postures[43,44,50] can also be combined with this framework. Technically, using wireless sensors, actuators and automated analysis can be considered a particular extension of the 'Internet of Things'[51]. Hence, hardware and software development from the Internet of Things field will most likely inspire the design of improved devices and enable better behavioral models and analysis methods.

Online content

Any methods, additional references, Nature Research reporting summaries, source data, extended data, supplementary information, acknowledgements, peer review information; details of author contributions and competing interests; and statements of data and code availability are available at https://doi.org/10.1038/s41592-020-0961-2.

Received: 16 September 2019; Accepted: 24 August 2020;
Published online: 29 September 2020

References

1. Tinbergen, N *The Study of Instinct 195* (Clarendon Press, 1951).
2. Krakauer, J. W., Ghazanfar, A. A., Gomez-Marin, A., MacIver, M. A. & Poeppel, D. Neuroscience needs behavior: correcting a reductionist bias. *Neuron* **93**, 480–490 (2017).
3. Huber, F. & Markl, H. (eds) *Neuroethology and Behavioral Physiology: Roots and Growing Points* (Springer, 1983).
4. Hölscher, C., Schnee, A., Dahmen, H., Setia, L. & Mallot, H. A. Rats are able to navigate in virtual environments. *J. Exp. Biol.* **208**, 561–569 (2005).
5. Dombeck, D. A., Harvey, C. D., Tian, L., Looger, L. L. & Tank, D. W. Functional imaging of hippocampal place cells at cellular resolution during virtual navigation. *Nat. Neurosci.* **13**, 1433–1440 (2010).
6. Keller, G. B., Bonhoeffer, T. & Hübener, M. Sensorimotor mismatch signals in primary visual cortex of the behaving mouse. *Neuron* **74**, 809–815 (2012).
7. Harvey, C. D., Collman, F., Dombeck, D. A. & Tank, D. W. Intracellular dynamics of hippocampal place cells during virtual navigation. *Nature* **461**, 941–946 (2009).
8. Minderer, M., Harvey, C. D., Donato, F. & Moser, E. I. Neuroscience: virtual reality explored. *Nature* **533**, 324–325 (2016).
9. Aghajan, Z. M. et al. Impaired spatial selectivity and intact phase precession in two-dimensional virtual reality. *Nat. Neurosci.* **18**, 121–128 (2015).
10. Aronov, D. & Tank, D. W. Engagement of neural circuits underlying 2D spatial navigation in a rodent virtual reality system. *Neuron* **84**, 442–456 (2014).
11. Stowers, J. R. et al. Virtual reality for freely moving animals. *Nat. Methods* **14**, 995–1002 (2017).
12. Dombeck, D. A., Khabbaz, A. N., Collman, F., Adelman, T. L. & Tank, D. W. Imaging large-scale neural activity with cellular resolution in awake, mobile mice. *Neuron* **56**, 43–57 (2007).
13. Sofroniew, N. J., Cohen, J. D., Lee, A. K. & Svoboda, K. Natural whisker-guided behavior by head-fixed mice in tactile virtual reality. *J. Neurosci.* **34**, 9537–9550 (2014).
14. Radvansky, B. A. & Dombeck, D. A. An olfactory virtual reality system for mice. *Nat. Commun.* **9**, 839 (2018).
15. Fry, S. N., Bichsel, M., Müller, P. & Robert, D. Tracking of flying insects using pan-tilt cameras. *J. Neurosci. Methods* **101**, 59–67 (2000).
16. Fry, S. N., Rohrseitz, N., Straw, A. D. & Dickinson, M. H. TrackFly: virtual reality for a behavioral system analysis in free-flying fruit flies. *J. Neurosci. Methods* **171**, 110–117 (2008).
17. Straw, A. D., Branson, K., Neumann, T. R. & Dickinson, M. H. Multi-camera real-time three-dimensional tracking of multiple flying animals. *J. R. Soc. Interface* **8**, 395–409 (2011).
18. Bath, D. E. et al. FlyMAD: rapid thermogenetic control of neuronal activity in freely walking *Drosophila*. *Nat. Methods* **11**, 756–762 (2014).
19. Romero-Ferrero, F., Bergomi, M. G., Hinz, R. C., Heras, F. J. H. & de Polavieja, G. G. idtracker.ai: tracking all individuals in small or large collectives of unmarked animals. *Nat. Methods* **16**, 179–182 (2019).
20. Weissbrod, A. et al. Automated long-term tracking and social behavioural phenotyping of animal colonies within a semi-natural environment. *Nat. Commun.* **4**, 2018 (2013).
21. de Chaumont, F. et al. Computerized video analysis of social interactions in mice. *Nat. Methods* **9**, 410–417 (2012).
22. Matsumoto, J. et al. A 3D-video-based computerized analysis of social and sexual interactions in rats. *PLoS ONE* **8**, e78460 (2013).
23. Ballesta, S., Reymond, G., Pozzobon, M. & Duhamel, J.-R. A real-time 3D video tracking system for monitoring primate groups. *J. Neurosci. Methods* **234**, 147–152 (2014).
24. Khan, Z., Herman, R. A., Wallen, K. & Balch, T. An outdoor 3-D visual tracking system for the study of spatial navigation and memory in rhesus monkeys. *Behav. Res. Methods* **37**, 453–463 (2005).
25. Tsoar, A. et al. Large-scale navigational map in a mammal. *Proc. Natl Acad. Sci. USA* **108**, E718–E724 (2011).
26. Yartsev, M. M. & Ulanovsky, N. Representation of three-dimensional space in the hippocampus of flying bats. *Science* **340**, 367–372 (2013).
27. Hong, W. et al. Automated measurement of mouse social behaviors using depth sensing, video tracking, and machine learning. *Proc. Natl Acad. Sci. USA* **112**, E5351–E5360 (2015).
28. Shemesh, Y. et al. Correction: high-order social interactions in groups of mice. *eLife* **3**, e03602 (2014).
29. De Chaumont, F. et al. Real-time analysis of the behaviour of groups of mice via a depth-sensing camera and machine learning. *Nat. Biomed. Eng.* **3**, 930–942 (2019).
30. Pérez-Escudero, A., Vicente-Page, J., Hinz, R. C., Arganda, S. & de Polavieja, G. G. idTracker: tracking individuals in a group by automatic identification of unmarked animals. *Nat. Methods* **11**, 743–748 (2014).
31. Strauss, R., Schuster, S. & Götz, K. G. Processing of artificial visual feedback in the walking fruit fly *Drosophila melanogaster*. *J. Exp. Biol.* **200**, 1281–1296 (1997).
32. Del Grosso, N. A., Graboski, J. J., Chen, W., Blanco-Hernández, E. & Sirota, A. Virtual reality system for freely-moving rodents. Preprint at *bioRxiv* https://doi.org/10.1101/161232 (2017).
33. Buccino, A. P. et al. Open source modules for tracking animal behavior and closed-loop stimulation based on Open Ephys and Bonsai. *J. Neural Eng.* **15**, 055002 (2018).
34. Lim, J. & Celikel, T. Real-time contextual feedback for close-loop control of navigation. *J. Neural Eng.* **16**, https://iopscience.iop.org/article/10.1088/1741-2552/ab2ffa (2019).
35. Stephens, D. W., Brown, J. S. & Ydenberg, R. C. *Foraging: Behavior and Ecology* (University of Chicago Press, 2008).
36. Krebs, J. R. & Davies, N. B. *Behavioural Ecology: An Evolutionary Approach* (John Wiley & Sons, 2009).
37. Silcox, M. T. & López-Torres, S. Major questions in the study of primate origins. *Ann. Rev. Earth Planet. Sci.* **45**, 113–137 (2017).
38. Grobéty, M.-C. & Schenk, F. Spatial learning in a three-dimensional maze. *Anim. Behav.* **43**, 1011–1020 (1992).
39. Jovalekic, A. et al. Horizontal biases in rats' use of three-dimensional space. *Behav. Brain Res.* **222**, 279–288 (2011).
40. Skinner, B. F. *The Behaviour of Organisms* (D. Appleton and Co., 1938).
41. Breland, K. & Breland, M. A field of applied animal psychology. *Am. Psychol.* **6**, 202–204 (1951).
42. Pryor, K. *Don't Shoot the Dog! The New Art of Teaching and Training* revised edn (Bantam Books, 1999).
43. Wiltschko, A. B. et al. Mapping sub-second structure in mouse behavior. *Neuron* **88**, 1121–1135 (2015).
44. Mathis, A. et al. DeepLabCut: markerless pose estimation of user-defined body parts with deep learning. *Nat. Neurosci.* **21**, 1281–1289 (2018).
45. Tsai, H.-C. et al. Phasic firing in dopaminergic neurons is sufficient for behavioral conditioning. *Science* **324**, 1080–1084 (2009).

46. O'keefe, J. & Nadel, L. *The Hippocampus as a Cognitive Map* (Clarendon Press, 1978).
47. Wilson, M. A. & McNaughton, B. L. Dynamics of the hippocampal ensemble code for space. *Science* **261**, 1055–1058 (1993).
48. Ulanovsky, N. Neuroscience: how is three-dimensional space encoded in the brain? *Curr. Biol.* **21**, R886–R888 (2011).
49. Finkelstein, A. et al. Three-dimensional head-direction coding in the bat brain. *Nature* **517**, 159–164 (2015).
50. Pereira, T. D. et al. Fast animal pose estimation using deep neural networks. *Nat. Methods* **16**, 117–125 (2019).
51. Gershenfeld, N., Krikorian, R. & Cohen, D. The internet of things. *Sci. Am.* **291**, 76–81 (2004).

Methods

Hardware. *Infrared real-time video tracking system.* Four to six high-speed USB3 cameras (MQ013CG-ON, XIMEA) were used for tracking. The cameras were equipped with wide-angle lenses (NAVITAR, f4.5 mm, 1.4) and infrared long-pass filters (FGL 665, Thorlabs, or 832 nm Bandpass Filter, Edmund Optics) to eliminate light in the visible range. Each camera was connected via a USB connection to an independent GPU-based microprocessor (Jetson TK1 or TX2, NVIDIA, running Linux4Tegra). The microprocessors communicated via ethernet (TK1) or WIFI (TX2) with a central host machine (Optiplex 9020, Intel Core i7, Dell, running Linux Ubuntu 16.04 LTS) using a wireless router (RT-AC88U, ASUS). An additional USB3 camera (MQCG-ON, XIMEA) was connected to the host machine for continuous monitoring of the experimental room. Cameras and GPU units could either be powered by external power supplies or with 12-V car batteries (44 ampere hours (Ah), Miocar). When tracking with passive reflective markers (see below), the tracking cameras were equipped with a custom illumination ring of 20 LEDs with wavelength of 850 nm (TSHG6400, Vishay Semiconductors).

Portable passive markers. Passive reflective markers consisted either of retro-reflective spheres (14 mm, Optitrack), or were custom made with flexible retro-reflective transfer foil (Seritec) in the shape of a neck collar.

Portable active markers. To track multiple animals simultaneously, infrared LED light sources of different wavelengths were used (SMC660, SMC750, SMC830, Roithner). These wavelengths are beyond the visible spectrum of mouse lemurs, and therefore do not interfere with their photoperiod[52]. To make the light spot visible from wide angles, the light was diffused using 6-mm opal glass diffuser (no. 46163, Edmund Optics). To hold the light sources on the top of the neck of the mouse lemurs, the animal carried a custom collar around its neck with a miniature rechargeable battery attached below (Lipo 3.7 V, 140 mAh, LP451430). The total weight of the neck collar including the battery was <4 g.

Close-up imaging system. The close-up imaging system consisted of a near-infrared enhanced CMOS camera (MQ013RG-E2, XIMEA), mounted on the center of a custom designed two-axis gimbal, actuated by two high-power digital servo motors (MX-64, Dynamixel). The camera was equipped with a high-resolution lens (Xenon, 2.0/50 mm, Schneider or a Rodagon, 4.0/80 mm, Rodenstock) and an electrically tunable lens (EL-16-40-TC, Optotune). According to the manufacturer's specification, the response time of this lens is ~7 ms for a square pulse of 0–250 mA. The central host machine was communicating in real time with the servos via a serial port protocol (USB2Dynamixel). The focus of the electrically tunable lens was simultaneously controlled via ethernet protocol and a dedicated controller (TR-CL180, GIGE Vision). For recordings with mouse lemurs, the close-up camera system was protected with a transparent Plexiglas half-dome (40 cm, Lacrylic shop).

Target illumination system. To illuminate animals for the close-up imaging system, a high-power infrared LED (H2W5, 850 nm) and reflector (10158, Roithner) or a narrow beam LED (ELJ-650-637, Roithner) was mounted in parallel with the close-up imaging system. Alternatively, the target illumination system was mounted separately on a second two-axis gimbal powered by two digital servo motors (MX-64, Dynamixel) and were controlled via a serial port (USB2, Dynamixel).

Remote-controlled stimulus and reward boxes (RECO box). The RECO box is based on a low-power WiFi-enabled microprocessor (MKR-1000, Arduino) powered by a lithium ion battery (3.7 V, 7.8 Ah, Pi-shop) and interacted via a wireless user datagram protocol (UDP) protocol with the host computer. The following parts were packed inside a waterproof plastic box ($100\times100\times90\,mm^3$, RND 455-00123, RND Component) and held in place by a custom 3D-printed insert. An optical lick port with a single lick spout was mounted on the top cover of the plastic box. Auditory stimuli (9 kHz tone) were generated by a piezo speaker (KPEG-126, Kingstate), and loud clicks by a solenoid valve (ZHO-0420L/S, Adafruit) tapping against the plastic side wall. A green LED (565 nm) was activated as a visual cue, whereas an infrared LED (750 nm) was used to localize the position of the RECO box by the tracking system. The liquid reward was stored in a 20-ml glass bottle and delivered to the lick port by a peristaltic pump (OINA). The stepper motor (QSH-2818, Trinamic) of the pump was controlled via a low-voltage stepper driver (DRV8833, Adafruit).

Software. EthoLoop software was written in C++ using OpenCV and CUDA libraries. Real-time 3D visualization of data points was done by gnuplot (www.gnuplot.info). Dynamixel SDK libraries for C++ were used to control the servos of the close-up system (www.github.com/ROBOTIS-GIT). RECO boxes were programmed with Arduino software (IDE).

Animals. *Mouse lemurs.* Four adult gray mouse lemurs (*M. murinus*) were used for this study (Supplementary Table 1). All mouse lemurs were born and raised in the 'Mouse Lemur Platform' (authorization number E-91-114-1) of the Museum of Natural History in Brunoy, France, under the supervision of the staff of the UMR CNRS-MNHN 7179-MECADEV. The procedures are in accordance with European animal welfare regulations and were reviewed by the local ethics committee (Comité d'éthique en expérimentation animale no. 68) in Brunoy, France, by the ethics committee of the University of Geneva, Switzerland, and authorized by the French 'Ministère de l'éducation nationale de l'enseignement supérieur et de la recherche'. All experiments involving mouse lemurs were carried out in Brunoy, France. The behavioral experiments were restricted to the awake period of their circadian cycle (dark). Animals were housed socially (2 or 3 per cage) in cages ($50\times60\times70\,cm^3$) with wooden branches, leaves and wooden nest boxes. Temperature was kept between 24 and 26 °C, relative humidity was approximately 55% and artificial light cycle was 14 h on per day (winter period[53]). Animals had free access to water and food consisting of pieces of fresh apples and bananas, insect larvae and a liquid food mix (condensed milk, egg yolk, cottage cheese, spice bread, baby milk powder diluted in water and homogenized in a kitchen mixer).

Mouse lemur experimental room. The experimental room for the mouse lemurs ($1.7\times2\times3.1\,m^3$) was covered with matt black paint to avoid reflections of the infrared light sources. The mouse lemurs were allowed to freely roam in the room. The lighting condition of the room was controlled in respect to the animals' day/night cycles and the temperature was maintained at 25 °C. For initial tracking sessions and social interactions, the experimental room was equipped with tree branches, food platforms and wooden nest boxes (one per animal) (Fig. 1). For closed-loop experiments, the room was equipped with a custom-made 3D lattice maze inspired by ref. [38]. The sides of the lattice cubes (500 mm) were built out of round wood and ranged in diameter from 4 to 24 mm.

During the days of the behavioral experiments, food availability was limited to the behavioral sessions to increase motivation. The weight and overall behavior of the animals was monitored twice a day. The animals were habituated to the RECO boxes in their home cages, where liquid food (described above) was available at random moments (on average every minute). Reward availability was indicated with an auditory cue (9 kHz tone approximately every minute) and delivery was triggered if a lick followed within 30 s. The conditioning experiments were usually stopped after the animals performed ~120 trials (reward size, ~0.02 ml of liquid food mix) or when they showed a drop in motivation (ignoring the task for >5 min). Additional food was supplemented after the experiment to keep the weight stable.

Mice. Ten laboratory mice (C57Bl/6J, Jackson Laboratory) were used for the conditioning experiments (six mice for open-field and four mice for the 3D arena). All experiments with mice were carried out in Geneva, Switzerland, and reviewed by the local ethics committee and authorities of the Geneva canton. Animal cages were kept in the animal facility (temperature of 21 °C and humidity of 50%) and each cage was housing a maximum of five mice. During behavioral experiments, access to water was restricted to the behavioral session and limited to 1 ml per day[54]. Mice were monitored daily and additional water was provided if necessary. All the experiments were carried out in the dark period of their circadian cycle. The conditioning experiments were stopped after the animals performed ~100 trials (reward size, ~0.01 ml of water) or when they showed a drop in motivation. Additional water was supplemented after the experiment to keep the weight stable.

Surgery for optogenetic stimulation. For optogenetic experiments using DAT-iresCre mice (Slc6a3$^{tm1.1(cre)Bkmn}$/J, called DAT-Cre in the manuscript), the animals were injected with rAAV5-Ef1a-DIO-hChR2(H134R)-eYFP (Addgene) in the VTA. Mice were anesthetized with a mixture of oxygen ($1\,l\,min^{-1}$) and isoflurane 3% (Baxter) and placed in a stereotactic frame (Angle One, Leica). The skin was shaved, locally anesthetized with 40–50 µl lidocaine 0.5% and disinfected. The animals were placed in a stereotactic frame and bilateral craniotomy was made over the VTA at the following stereotactic coordinates: lateral ±0.5 mm, posterior −3.2 mm, depth −4.20 ± 0.05 mm from Bregma. A total volume of 500 nl was injected. The virus expressed for 3–4 weeks and mice were subsequently implanted with optic fibers (200 µm, ThorLabs, for the tethered experiments) or with a custom fiber-coupled (400 µm, FP400URT, Thorlabs) miniature LED (OVS5MBBCR4, TTI) wired to a miniature connector (Millmax). To deliver the light via the optical fibers to the DA neurons, the VTA was targeted with a 10° angle at the following coordinates: lateral ±0.9 mm, posterior −3.2 mm, depth −3.95 ± 0.05 mm from Bregma. The fibers were fixed on the skull with dental acrylic. The placement of the optical fiber and the range of virus infection were confirmed post hoc immunostaining (Supplementary Fig. 7). We used a primary antibody against Tyrosine Hydroxylase (TH, 1/500 dilution) enzyme, followed by secondary antibody donkey anti rabbit alexa fluor 555 (1/500 dilution).

Experimental procedures. *Optical tracking and 3D reconstruction.* The local processing of the images of the tracking cameras on the NVIDIA Jetson TX2 consisted of several steps carried out in multiple parallel threads:

(1) Adjusting camera parameters: XIMEA camera parameters such as exposure, gain, downsampling, image format and sensor's bit depth were initially adjusted. Setting the exposure level to <1.2 ms, downsampling by 2×2 (pixel skipping method, final resolution is 640×512), retrieving frames in RAW 8-bit format and enabling ZERO-ROT mode allowed us to achieve a maximum performance of ~780 frames per second. The communication

with the camera for grabbing and retrieving frames is done in parallel central processing units threads to minimize latency and maximize tracking speed (Supplementary Fig. 2).

(2) Custom color demosaicing: to spectrally separate the hues of different infrared LEDs, we developed a custom demosaicing process using OpenCV and CUDA libraries (Supplementary Fig. 3). The ratio of the different color sensitivity curves (specified by the camera chip, OnSemi PYTHON 1300) were used as a lookup table to produce the false colors. This process resulted in a mapping of 660 nm to visible red, 750 nm to orange and 810 nm to blue.

(3) 2D target position estimation: the different colors were thresholded by pre-specified values for hue, saturation and value, and the centroid of the target image blob was estimated by a projection barycenter algorithm[23].

(4) Communication with the central host computer: The 2D position of the centroids determined by each tracking camera per GPU was sent to the central host computer via the network using the UDP protocol.

The triangulation of the simultaneously received 2D target information was performed in the central host computer by using a projective-invariant method, whereby the 3D target position was chosen to minimize the quadratic distance between its computed 2D projections and the measured 2D targets[23,55,56]. Correct triangulation of a 3D target is theoretically possible when seen by at least two cameras. However, robustness to image noise and visual occlusions increases with the number of available cameras in the setup. In practice, 4–6 cameras were found to be sufficient to cover a 10-m^3 room with branches. The actual spatial resolution of the tracking does not depend on the number of cameras, but is defined primarily by the resolution and optics of the cameras, their position relative to the targets and the quality of the spatial calibration of the system.

Calibration of the 3D tracking system. An initial geometric calibration phase of the system was performed by manually moving a single LED target over the entire measurement space. The recorded 2D projections were first used to estimate the 3D position of the first two cameras using the five-point algorithm[57] and RANSAC estimation methods implemented in OpenCV. The 3D target position was then reconstructed using the above-mentioned triangulation algorithm. The position of each additional camera was then estimated with OpenCV's implementation of the perspective-n-point algorithm[57] using the 3D triangulated points. The resulting estimated position of all cameras was then refined, using a bundle adjustment method based on a sparse Levenberg–Marquardt optimization procedure, as implemented in the SSBA software library[58]. As usual for 3D reconstruction algorithms, a final calibration was done to align and scale the resulting data to real-world coordinates, using a reference box object of known dimensions placed in the measurement space.

To illustrate the ability of the EthoLoop system to track fast-moving objects in large-scale environments (>100 m^3), a commercial drone (Tello by DJI, Ryze Tech) was used (Supplementary Fig. 1 and Supplementary Video 4). The drone was steered around the plants in the room under manual control.

Calibration of the close-up system. The liquid lens autofocus of the close-up system was calibrated manually by placing an object at more than four locations in front of the camera while adjusting the necessary current to achieve perfect focus. These settings were used to fit a current–distance curve for the tunable lens.

The spatial parameters of the close-up system were calibrated using a semi-automated procedure. An infrared LED was placed at a random location and the close-up system started to scan the environment by spinning over the axes of both servos while capturing RAW images and thresholding in a specific range of the infrared LED (60 frames per second at full resolution of 1,024×1,280). This scanning stopped as soon as the LED was detected by the camera. At this point the close-up system started to move in steps of 0.087° (in both axes of servos) every 500 ms to locate the LED at the center of the frame. The exact 3D position of the LED calculated by the host machine (x,y,z), and the final angle of both servos (azimuth α, elevation β) were saved. The procedure was repeated several times, and the location x_c,y_c,z_c of the close-up camera was computed by solving the system of equations:

$$\tan(\beta) = \frac{x - x_c}{y - y_c}$$

$$\tan(\alpha) = \frac{z - z_c}{\sqrt{(x - x_c)^2 + (y - y_c)^2}}$$

Finally, the angles of the servo motors were trigonometrically calculated by the host machine based on the spatial position of the target and respective location of the close-up camera and communicated via the serial port. In parallel, the distance from the target to the close-up camera was calculated and sent via ethernet to the GIGE Vision controller to focus the tunable lens on the object using the above-mentioned calibration curve.

Evaluation of EthoLoop system performance. *3D tracking and real-time behavior analysis latency.* The latency for 3D tracking was defined by the time between the appearance of a target and the 3D reconstruction. To measure this latency, a microcontroller (Arduino Mega) with an infrared LED (750 nm) was connected to the host PC and placed in the tracking area. The host program was modified to command the microcontroller to illuminate the LED at repeated intervals, and to measure the time elapsed until reception of the corresponding 3D position measurement of the LED. This procedure was repeated 1,000 times at random intervals. The average value gives a high estimate of the actual latency of the system, considering the added latency of commanding the microcontroller to turn on the infrared LED (Fig. 1b and Supplementary Fig 2).

The latency of the real-time behavioral analysis was defined by the time evolving between turning on a LED in the field of view of the close-up system, its correct identification by the DeepLabCut software (with pretrained network) and the final receipt by the host computer of the 2D coordinates (position of the LED within the close-up image) and likelihoods of correct identification (Fig. 1b). The procedure for turning on the LED and calculating the time difference was identical to the one described above (tracking latency).

RECO box communication latency. The latency to communicate with a RECO box was defined as the time between sending a command (by the host machine) and the reception of that command by the RECO box. For this purpose, 1,000 commands at random intervals were sent to a RECO box to turn on the infrared LED. Once the LED was turned on, the cameras sent the 2D coordinate to the host machine for 3D reconstruction. The time difference between sending of the command and the reconstruction of the LED's 3D position was calculated by the host machine. These measurements were then subtracted from the mean value of 3D reconstruction latency (single target, Fig. 1b, light-red histogram) to obtain communication latency with the RECO box (Fig. 1b, blue histogram).

Rate of 3D tracking and real-time behavior analysis. The interval for 3D tracking was defined as the time between two subsequent 3D reconstructions. We recorded the time between reception of subsequent 3D data measurements, repeated over a 60-s tracking session with one, two and three targets (Fig. 1c). Real-time behavior analysis interval was defined as the time between subsequent detection and labeling of body parts. For this purpose, a moving doll was placed in front of the close-up camera. The body parts were labeled with the real-time DeepLabCut (using the pretrained network) and the time between subsequent labeled frames were recorded over 60 s.

Positional accuracy. An infrared LED was placed on the edge of a circular turntable (Thorens, TD160) spinning at 33 and 45 rounds per minute. The measurement was carried out in our large >10-m^3 tracking arena. The tracking cameras were therefore >2 m from the target. In this setting (resolution of 640×512) one pixel covered roughly 7×9 mm^2. The LED light source consisted of an actual tracking target including the 5-mm flat glass diffuser. The difference between the actual turntable radius and the radius of the circle of the trajectory tracked by the EthoLoop system was reported as the positional error estimated for the tracking system. The tracking error measured (<8 mm) was in the range of the actual target dimensions (Supplementary Fig. 1i).

Real-time detection of behaviors. To detect specific behaviors (rearing, Fig. 4) in the stream of close-up images the following steps were carried out:

(1) Real-time classification of body parts. The close-up images were labeled on-the-fly using a custom-programmed real-time version of DeepLabCut software[44]. Close-up images were initially streamed at full resolution (1,280×1,024) to a computer (Dell, Optiplex 990-Intel Core i7, equipped with a GeForce GTX 1080 Ti graphics card), resized to 640×512 and saved using OpenCV functions. In parallel, the images were further resized to 320×256 (to reduce latency and increase speed) and labeled by the DeepLabCut software. The deep neural network used for the classification was trained with hand-annotated images (<400 frames) from previous recordings carried out under identical lighting conditions. The tracked body parts included: eyes, nose, forelimbs, hind limbs and the base of the tail.

(2) Once the body parts were labeled in an image, the frame number, the coordinates of the body parts and their likelihood were saved in a single string. This string was transmitted in real-time as a UDP packet to the main host machine. A special thread in a multithreaded tracking program was assigned to receive and parse the string.

(3) Real-time detection of posture: the spatial relationship of individual real-time labeled body parts was used to define a given posture (Fig. 4a). Specifically, rearing was detected if one of the following conditions were met:

(a) Difference between the nose and hind limbs on the y axis was more than 200 pixels and both lines connecting the nose to the hind limbs made an angle of less than 20° with the y axis.

(b) Difference between one of the eyes and hind limbs in y axis was more than 200 pixels and both lines connecting one eye to the hind limbs made an angle of less than 20° with the y axis.

(a) **Spatial constraints**: in the experiments where the posture had to be carried out at a specific location (Fig. 4b–g), a predefined virtual sphere (200 mm) was placed at a chosen location. The reward was only triggered when the posture was detected within the sphere.

Real-time control of RECO box. The RECO box was controlled via a Wifi Arduino. After establishing the connection to the central host computer via the wireless network, the Arduino was waiting for incoming UDP packets. Each received packet was decoded and the corresponding function (reward, noise and so on) was activated. The delay of this process was around ~2.5 ms (Fig. 1b, blue histogram). The RECO boxes were attached to different branches of the lattice maze, and their position was determined by the tracking system using a built-in infrared LED (750 nm). RECO boxes indicated the availability of a reward as a 1-s long sound at 9 kHz repeated at 0.5 Hz. The actual reward was delivered on arrival of the animal within 10 cm of the RECO box.

Close-loop behavioral experiments. *Mouse lemur foraging.* Four to five RECO boxes were distributed at different locations inside the 3D lattice maze (Fig. 2 and Extended Data Fig. 1). Their activation was set in either predefined or random sequences. In experiments with defined sequences, a subsequent RECO box was activated when the animal reached a distance of 20 cm from the previous one. In experiments with random activation, a different RECO box was chosen at random to be activated after a variable delay (0 to 60 s) as soon as the animal reached a distance of 1 m to the previous activated box. In both cases, the animal was given 40 s to collect the reward from the active feeder.

Mouse lemur 3D place conditioning. On the entrance of the animal to a 15-cm radius sphere surrounding the selected location (place) a RECO box was activated. The animal was given 20 s to collect the reward from the active RECO box.

Mouse lemur behavioral conditioning (rearing). On executing the defined behavior (rearing) at a specified location a RECO box was activated. The animal was given 30 s to collect the reward from the active RECO box.

Mouse place conditioning. A RECO box was placed in an arena covered with tree branches (Fig. 3a–d and Extended Data Figs. 2a and 5a) or in an open-field (Extended Data Fig. 3a). The RECO box was localized by the tracking system with an infrared (750 nm) LED. The activation of a feeder was signaled by a click sound, and liquid reward (0.01 ml of 0.1% sucrose in water) was provided on arrival near the RECO box. Initially, the mice were habituated to the RECO box, by providing rewards at random intervals.

Mouse behavioral conditioning (rearing). To detect rearing on hind limbs, a threshold on the *z* axis was defined for mice performing the task in a simple 2D environment where they had to rear on an elevated platform (Extended Data Fig. 6). For mice performing the task in naturalistic 3D environment rearing was the same as described in Fig. 4a. Once rearing was detected, a RECO box was activated and the mouse had 10 s to collect the reward. If mice did not spontaneously rear on the defined location, a small bell was suspended by a string from the ceiling (pointing toward the rearing location). Mice rapidly started rearing to explore the new object. The bell was removed after the tenth rearing.

Wireless mouse optogenetic place and behavioral conditioning. The wireless optogenetic activation of the VTA in mice in the naturalistic arena was carried out using a portable, remote-controlled stimulation device (Supplementary Fig. 6). The unit was composed of the electronic circuit board ($16 \times 20\ mm^2$) taken from a miniature remote-controlled car (Nano Racer, Carson). The two leads originally powering the DC-motor were connected to the head mounted LED-fiber assembly targeting the VTA (see details above). The unit was powered by a rechargeable 3.7-V lithium ion coin battery (CP 1254 A3, Varta) and attached around the neck of the mouse for the duration of the experiment. The optogenetic stimulation consisted of 8 × 20-ms pulses repeated at 10 Hz. The power output at the end of the fiber was ~5 mW. To control the timing of the pulses, the original remote control was connected to a WiFi-enabled microprocessor (MKR-1000, Arduino) circuit that received the commands wirelessly via a UDP protocol from the host computer.

Fiber-based mouse optogenetic place and behavioral conditioning. For the optogenetic conditioning experiments on an open-field arena the mice were connected to a flexible optical fiber (FC/PC 200-µm fiber, 2 m, ThorLabs) hanging from the ceiling. The light source was a fiber pig-tailed to a blue laser (473 nm, 50 mW, OBIS, Coherent) controlled via a WiFi-enabled microprocessor (MKR-1000, Arduino) circuit. The maximal power of the fiber output was 20 mW (measured in continuous mode using a power meter (Field Mate, Coherent)). Stimulation consisted of eight pulses of 4-ms duration, repeated at 30 Hz (output ranging from 8–12 mW). During the place conditioning experiment, mice were optogenetically stimulated on entering the defined location (20–25-cm radius). The optogenetic stimulation continued for a maximum of eight consecutive bursts if the mouse remained inside the target area. The place conditioning experiments were stopped after the animals received ~900 burst stimulations. During the behavioral conditioning experiments, mice were optogenetically stimulated on executing the defined behavior (rearing) detected with the real-time DeepLabCut software. The experiments were stopped after the animals received ~450 burst stimulations.

Mouse lemur electrophysiological recordings. *Electrodes and drive.* Custom-made tetrode wire bundles were produced by twisting and heating four individual 12.7-µm Tetrode Nickel-Chrome Wires covered with Easy Bond XTC (Sandvik). Tetrodes were inserted and glued into polyamide tubing (0.14-mm diameter) inside the moving part of a custom designed 3D-printed microdrive. The electrode tips were cut and gold-plated with Sifco 5355 (mixed 1:1 with polyethylene glycol solution and carbon nanotubes, Neuralynx) to lower the impedance. The free end of the tetrode was connected to a miniature connector (Omnetics) via a custom designed interface board. The tetrode array was lowered by turning the M1 screw of the microdrive.

Electrophysiology setup. Extracellular recordings were performed using custom wireless data acquisition logger hardware (Spike Gadgets) together with Trodes software (Spike Gadgets). Acquired data were sampled at 20 kHz and broad-band filtered between 0.1 Hz and 10 kHz. Data were further filtered post hoc between 600 Hz and 6 kHz for spike extraction. Spike sorting was carried out with semi-automated SpikingCircus and Kilosort algorithms.

Surgery. One day before the surgery the animal was administered antibiotics (Ceftriaxon, $50\ \mu g\ g^{-1}$, intramuscular) and housed individually without food. Surgeries were carried out under aseptic conditions. Anesthesia was induced in a small Plexiglas box with a continuous flow of a mixture of oxygen with 5% Isoflurane (Vetflurane, Virbac). After induction, the animal was removed from the box and placed in a custom designed stereotactic frame. Eyes were protected with Lacryvisc cream and whiskers and tongue were covered with Vaseline. Isoflurane was decreased (2.5–1%) while breathing rate and toe pinch reflexes were continuously monitored. The following drugs were administered: bupremorphine ($3\ \mu g\ g^{-1}$, subcutaneous), dexamethasone ($0.8\ \mu g\ g^{-1}$ intramuscular), ceftriaxon ($50\ \mu g\ g^{-1}$, intramuscular), carprofen ($22\ \mu g\ g^{-1}$, intramuscular) and rapidocaine (100–150 µl, locally injected). The area of the surgical procedure was disinfected sequentially with 70% ethanol, betadine and chlorhexidine 1%. The cranial bones were exposed after skin incision. The periosteum was gently removed with cotton swabs and the skull surface was dried and roughened to improve glue bonding. The area for the craniotomy was located at 0.5 mm anterior and 3 mm lateral from the interaural midpoint and was chosen based on coordinates from atlases of the mouse lemur brain[59–61]. A thin layer of cyanoacrylate (5011, ERGO) was applied on the skull and holes for ground wires and craniotomy for electrodes were made using a dental drill. The microdrive was placed on the skull and fixed with dental acrylic (Lang Dental). The skin was closed with stitches and the animal was placed on a heating blanket for recovery. Animals were monitored daily and administered with bupremorphine (analgesic, $3\ \mu g\ g^{-1}$, subcutaneous) for the following week and antibiotics (ceftriaxon ($50\ \mu g\ g^{-1}$, intramuscular) for a total of 9 d.

Synchronization of electrophysiology and tracking. To synchronize the 3D position from the tracking system and the electrophysiology recording, a signal was sent from the 3D tracking program to a Wifi Arduino (MKR-1000) via the UDP protocol. The timing of this signal was recorded in the tracking software. On arrival of the UDP packet at the Wifi Arduino, a digital pulse was sent to the main control unit of the electrophysiology acquisition system (Spike Gadgets) that synchronizes the recordings in the wireless head-stage via radio frequency pulses. The timings of these pulses were extracted offline and aligned with the 3D tracking.

Post hoc data analysis. All the position data, timing and signals (stimulations and rewards) were stored in a text file. All post data analysis was done in R using OpenGL libraries (www.r-project.org).

Position data filtering. Image artifacts produced by reflections can cause false detections in the 3D tracking system. These false detections appear as sudden jumps between the actual location of the LED and the reflecting surface. To correct for these artifacts:

- Points that appeared outside the tracking boundary were excluded.
- Sudden jumps (speed $>5\ m\ s^{-1}$) inside the tracking space were excluded and the trajectories interpolated.
- Finally, the tracking data was smoothed over all three axes using locally weighted regression (LOWESS function in R).

From the filtered position data, velocity and acceleration on each axis at each time point was computed using a moving average over a 60-ms sliding window.

Movement categorization (ethograms). Five behavioral types were automatically extracted from the animal's movements using the following mutually exclusive rules:

- 'Short quiet': velocity was below $20\ cm\ s^{-1}$ for less than 2 s.
- 'Long quiet': velocity was below $20\ cm\ s^{-1}$ for more than 2 s.
- 'Running': velocity was above $20\ cm\ s^{-1}$, and cumulative displacement was over 10 cm otherwise categorized into the above 'quiet' states, depending on duration.

- 'Jumping': vertical acceleration equal to Earth's gravity ±3 m s^{-2}.
- 'Falling': vertical acceleration equal to Earth's gravity ±3 m s^{-2}, vertical displacement above 20 cm and the average horizontal velocity below 50 cm s^{-1}.

Distance between animals during quiet states. In tracking sessions with two animals, when both animals were at long quiet state, we computed the 3D distance between them and the amount of time they were at this distance. A histogram of distances binned at 20-cm intervals was plotted where the *y* axis represents the percentage of time spent at each interval.

State transitions. State transitions were defined by the event when a lemur changed from one state to another state. The distances between two mouse lemurs were calculated when one of them (lemur A) transitions from 'long quiet' to 'running' state ($ST_{Q\to R}$) while the other animal was in 'running' state (lemur B). These distances were all binned in 200 mm intervals and the number of $ST_{Q\to R}$ at each interval was calculated. At each distance interval, the probability of $ST_{Q\to R}$ of lemur A on approaching lemur B was estimated as the number of $ST_{Q\to R}$ divided by the total duration where distance between two animals was within the interval. To detect whether lemur B was approaching lemur A or moving away, the distance between them was also calculated 2 s before $ST_{Q\to R}$ of lemur A.

Analysis of closed-loop experiment with RECO box. In the closed-loop experiments using RECO box (place and behavior conditioning in mice and mouse lemurs) the time until the animals activate the RECO box for the 50th time by entering conditioned location or executing the conditioned behavior was divided into three equal time bins termed beginning, middle and end.

Analysis of the operant conditioning by optogenetic stimulation. In the place conditioning sessions, the time until the first 50th entrance to the conditioned place and in the behavioral conditioning session the time until the first 100 rearings was divided into three equal time bins termed beginning, middle and end.

3D reconstruction of lattice maze. All 60 cubes connecting different branches of the lattice maze were numbered. Each branch in the lattice maze was defined by its thickness (4, 6, 12 and 24 mm) and the cube numbers connecting them to each other. The 3D coordinate of the first cube was manually measured in the real-world coordinates and set as the base for reconstructing the lattice maze in 3D. The 3D position of all cubes in the lattice maze was reconstructed relative to the base cube (considering the constant 3D distance between neighboring cubes). Finally, the whole lattice maze was reconstructed by adding the branches while knowing their connecting cubes.

Analysis of electrophysiology. Spike rates (for the color-coded trajectories in Fig. 6a,c,e) were calculated by averaging the number of spikes during a sliding window (500 ms). The trajectories of the mouse lemurs were divided into bins of 13 cm displacement length. Spike rates were assigned to each bin by counting the number of spikes divided by the time taken to complete the displacements. The floor (Fig. 6b) was defined as the first 30 cm above ground.

For cells with spatially restricted firing, a virtual 10-cm sphere was initially placed at the center of the branch. All passages through the sphere with their respective firing rate were aligned based on their minimum distance to the center of the sphere (time zero is when the minimum distance happens for each passage, Fig. 6d). Iteratively, the sphere was moved along the branch and the firing rate of all trajectories were calculated and aligned. The sphere movement was stopped once the average firing rate of all trajectories reached its maximum value when passing the center of the sphere. This center of the sphere at this location was considered to be the center.

For a more detailed analysis (Fig. 6e–j), the direction of displacement was also added as a factor, creating directional vectors. The vectors were color-coded based on the spike rate and the thickness of branches (4 and 6 mm considered as thin, and 12 and 24 mm considered as thick). To quantify the movement along branches, the area around the connecting cubes (radius of 5 cm) were excluded from this analysis. The nomenclature of the directions (north, south, east, west, up, down) were defined with regards to the *x*, *y* and *z* axis of the lattice maze and independent of the real-world coordinates.

In vivo estimation of tetrode position in the mouse lemur brain. The position of the tetrode bundles was determined by the 3D reconstruction of computer tomography scans acquired in the anesthetized animals (isoflurane, as detailed above, scan time, 3 min), which were carried out at the MicroCT platform of Paris Descartes University. The position of the brain areas with respect to the skull and the tetrodes (reconstructed by the computer tomography data) were estimated based on the manual alignment of existing data from high-resolution MRI atlas[61], Supplementary Fig. 7) using the AMIRA software (Thermo Fisher Scientific).

Statistics and reproducibility. All the statistical analysis was carried out using R. A two-sided two-sample Kolmogorov–Smirnov test was used to compare distributions in Extended Data Figs. 1g and 6b. For all one-way repeated measure analysis of variance (ANOVA) tests, Mauchly's test was used to test the sphericity assumption and the Shapiro–Wilk test was performed to test the normality assumption (Figs. 3d, 4e and 5e,i and Extended Data Figs. 3b and 7b). A pairwise *t*-test was performed as post hoc analysis with the Bonferroni correction for multiple comparison. For the analysis of the directional-branch related cell (Extended Data Fig. 8) we performed two independent nonparametric one-way ANOVA tests (Kruskal–Wallis test), since both assumptions of normality and homogeneity of variance were not met.

Reporting Summary. Further information on research design is available in the Nature Research Reporting Summary linked to this article.

Data availability

The MRI Atlas for the mouse lemur is available at https://www.nitrc.org/projects/mouselemuratlas. Source data for Figs. 1 and 3–6 as well as source data for Extended Data Figs. 1–3, 6, 7 and 10 are provided. The original raw data containing all 3D trajectories, feedback signals and electrophysiology data is only available upon request due to the large file sizes. Source data are provided with this paper.

Code availability

All the codes for tracking (GPU units and host machine), RECO boxes and real-time labeling of body parts are available at www.huberlab.org/EthoLoop/software. R codes used for analysis are available upon request.

References

52. Perret, M., Gomez, D., Barbosa, A., Aujard, F. & Théry, M. Increased late night response to light controls the circadian pacemaker in a nocturnal primate. *J. Biol. Rhythms* **25**, 186–196 (2010).
53. Perret, M. Change in photoperiodic cycle affects life span in a prosimian primate (*Microcebus murinus*). *J. Biol. Rhythms* **12**, 136–145 (1997).
54. Guo, Z. V. et al. Procedures for behavioral experiments in head-fixed mice. *PLoS ONE* **9**, e88678 (2014).
55. Harltey, A. & Zisserman, A. *Multiple View Geometry in Computer Vision* (Cambridge Univ. Press, 2006).
56. Hartley, R. I. & Sturm, P. Triangulation. *Comput. Vis. Image Underst.* **68**, 146–157 (1997).
57. Nistér, D. An efficient solution to the five-point relative pose problem. *IEEE Trans. Pattern Anal. Mach. Intell.* **26**, 756–777 (2004).
58. Zach, C. Robust bundle adjustment revisited. In *Proc. Computer Vision – ECCV 2014 772–787* (Springer, 2014).
59. Bons, N. *A Stereotaxic Atlas of the Grey Lesser Mouse Lemur Brain (*Microcebus murinus*)* (Elsevier, 1998).
60. Dhenain, M., Ruffins, S. W. & Jacobs, R. E. Three-dimensional digital mouse atlas using high-resolution MRI. *Dev. Biol.* **232**, 458–470 (2001).
61. Nadkarni, N. A., Bougacha, S., Garin, C., Dhenain, M. & Picq, J.-L. Digital templates and brain atlas dataset for the mouse lemur primate. *Data Brief* **21**, 1178–1185 (2018).

Acknowledgements

We express our gratitude to the members of the Huber laboratory for their support and discussions. We thank M. Perret and the animal caretakers at the Brunoy facility for their help with mouse lemur breeding, care and handling, and H. Clamouze for constructing the maze. M. Scharter for advice with implementing DeepLabCut. We thank P. Yger for advice on spike sorting, L. Slimani and N. Liaudet for their help with the reconstruction of the electrode position. We thank Varta Microbattery for supplying the CP 1254 A3 coin batteries. We thank M. Prsa, G. Galiñanes and M. Long for their comments on the manuscript. This work was supported by the Vahabzadeh Foundation (A.N.), Human Frontiers Science Program (D.H. and F.P., grant no. RGP0024/2016), the New York Stem Cell Foundation (D.H.), Swiss National Science Foundation/Deutsche Forschungsgemeinschaft (D.H., grant no. 310030E_190060). D.H. is a New York Stem Cell Foundation-Robertson Investigator.

Author contributions

A.N. and D.H. conceptualized the EthoLoop system. A.N. and D.H. designed the tracking and close-up hardware. A.N. wrote all software for acquisition, tracking, close-loop control and RECO boxes. A.N. ran all experiments and analyzed all the data. D.H. oversaw data analysis. A.N., D.H. and S.P. designed the RECO box. R.Z. carried out the surgeries and ran the electrophysiological recording experiments. A.H. reconstructed the electrode trajectories. C.P.S. provided the mice and advice for the optogenetic experiments. Y.O. participated in the limb tracking. F.P. and F.A. provided expertise, guidance and resources related to the mouse lemurs. A.H. provided the 3D lattice maze and advice regarding the computer tomography scan. G.R. provided expertise for the tracking software. D.H. and A.N. wrote the manuscript.

Competing interests

The authors declare no competing interests.

Additional information

Extended data is available for this paper at https://doi.org/10.1038/s41592-020-0961-2.

Supplementary information is available for this paper at https://doi.org/10.1038/s41592-020-0961-2.

Correspondence and requests for materials should be addressed to D.H.

Peer review information Nina Vogt was the primary editor on this article and managed its editorial process and peer review in collaboration with the rest of the editorial team.

Reprints and permissions information is available at www.nature.com/reprints.

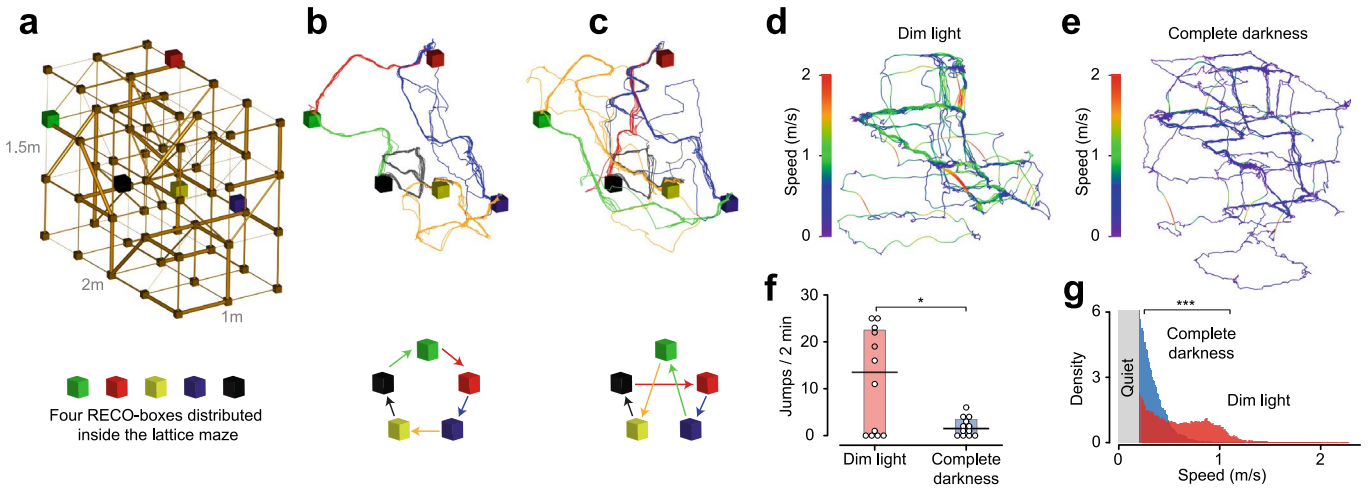

Extended Data Fig. 1 | Foraging mouse lemur in the lattice maze with 5 RECO-boxes. a, Five RECO-boxes (colored cubes) were spatially distributed at different locations of the lattice maze. RECO-boxes were activated in different sequences. **b**,**c**, Ten minutes of 3D trajectory of the mouse lemur where the RECO-boxes are activated in a circular (**b**) or non-circular order **(c)**. The trajectory color is based on the currently activated RECO-box. **e**,**f**, Speed of locomotion (color-coded) under dim light (**e**) and complete darkness **(f)**. **g**,**h**, The number of jumps (**g**) (12 time intervals for 1 mouse lemur, two-sided Wilcoxon signed rank test, **P*=0.0207) as well as the overall speed **(h)** was reduced in the absence of light (blue) compared to the dimly lit condition (red, two-sample Kolmogorov-Smirnov test, two sided, ****P*< 2.210-16). The boxplot in **(g)** represents the upper and lower quartiles as well as the median.

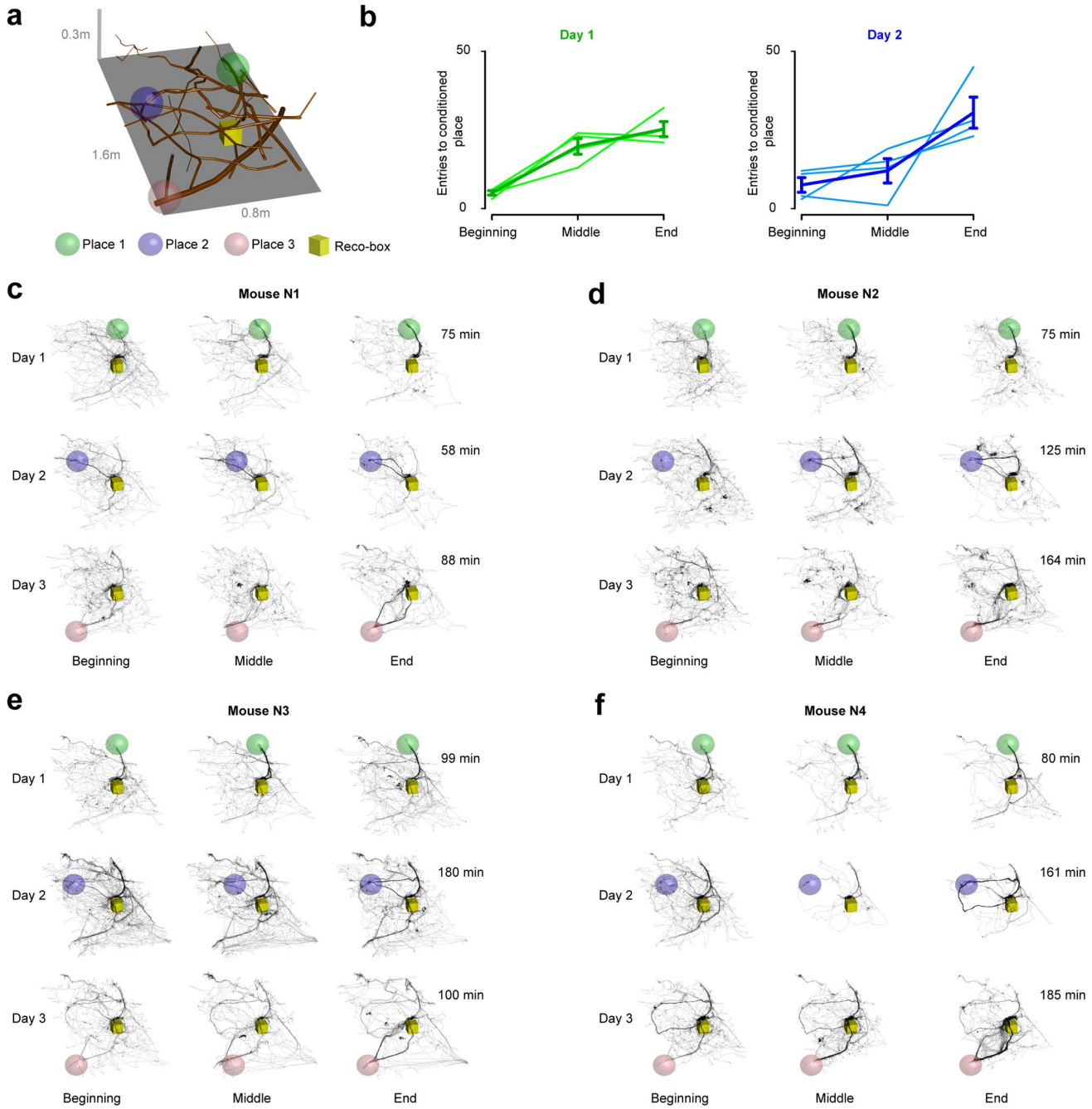

Extended Data Fig. 2 | Mouse place-conditioning in naturalistic conditions. a, The behavioral arena was filled with tree branches and included a RECO-box (yellow cube). Mice were conditioned to visit one of three unmarked locations (colored spheres). **b**, Number of entries to the conditioned place 1 and 2 during each session for all mice (N=4). Bars represent standard error of mean. **c**–**f**, 3D trajectories of the beginning, middle and end of all sessions for all four mice that underwent 3D place conditioning. Trajectories of Day 3 for Mouse N3 shown in Fig. 3b is repeated here. Three different conditioned locations are shown in green, red and purple spheres. The time to reach the criteria condition (50th entrance to the conditioned place) is noted on the right.

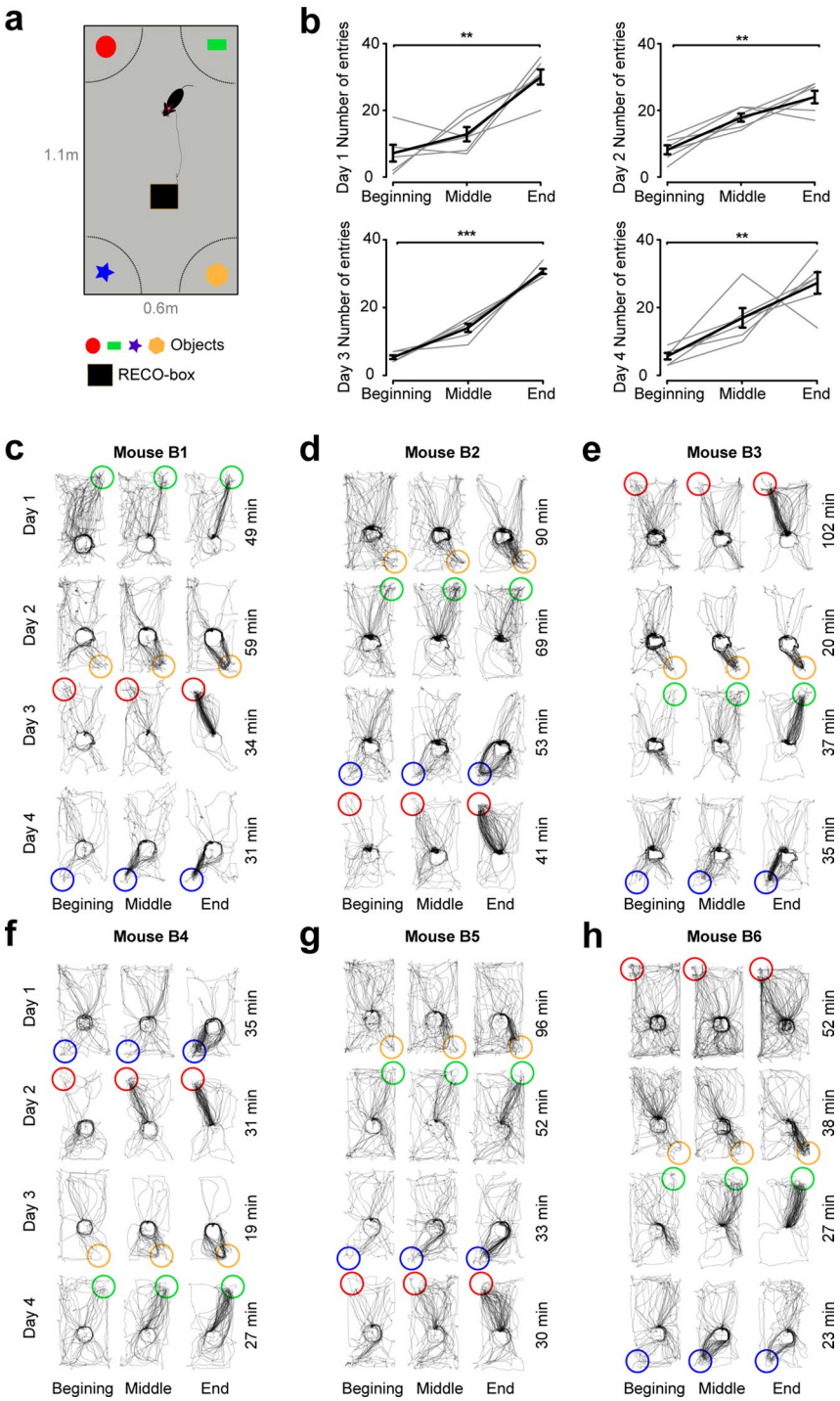

Extended Data Fig. 3 | Mouse place-conditioning in an open-field arena. a, A flat open-field arena for freely moving mice containing a single RECO-box and differently shaped objects placed at the four corners. The mice were trained to visit one of the four corners of the arena. Every session a different corner was reinforced. **b**, Number of entries to the conditioned place for all four days of training. For all days the mice entered the conditioned place more frequently (N= 6 mice; one-way repeated measure ANOVA; Two-sample pairwise t-test; Bonferroni correction for multiple comparison; beginning versus end; Day 1: ** P=0.009, Day 2: ** P=0.008; Day 3: *** P=2.910-7; Day 4: P=0.006). Error bars represent SEM. **c**–**h**, Original tracking traces of the beginning, middle and end of all sessions (four corners - illustrated with colored circles) for all six mice that underwent place conditioning. The time to reach the criteria condition (50th entry) is noted on the right.

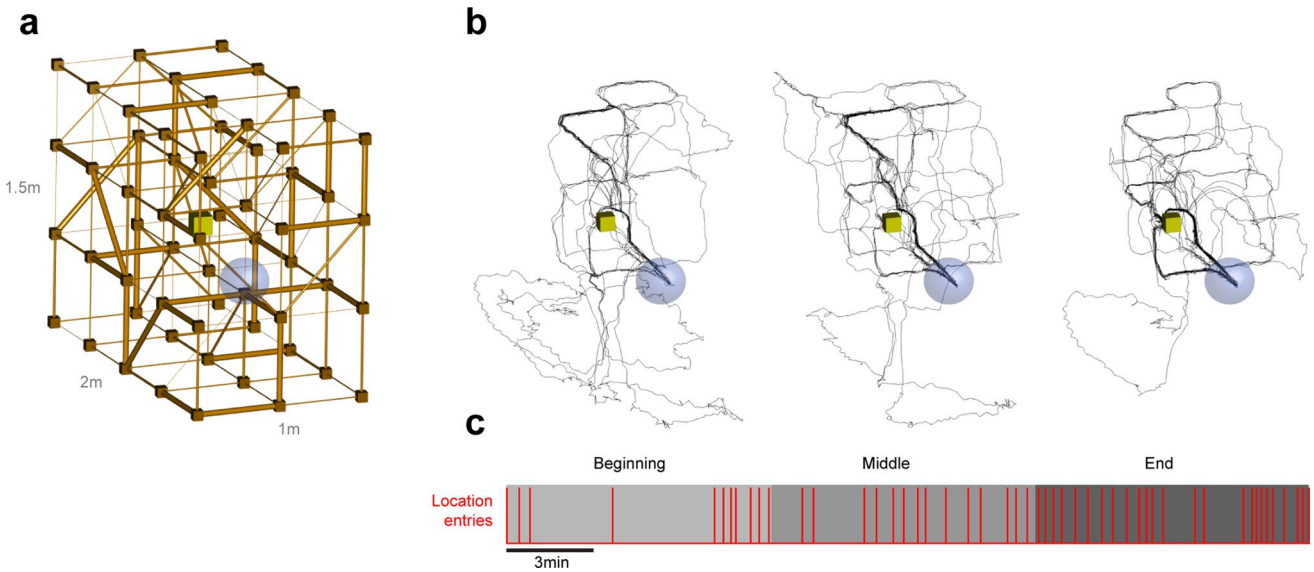

Extended Data Fig. 4 | Trajectory of a mouse lemur during a place-conditioning experiment in the lattice maze. a, Traces of a second conditioning experiment of a mouse lemur in the 3D lattice maze at the beginning, middle, and end of a behavioral session. The blue sphere indicates the location which was conditioned. **b**, The number of entries to the conditioned place across a behavioral session. **c**, Entries to the conditioned place across the session.

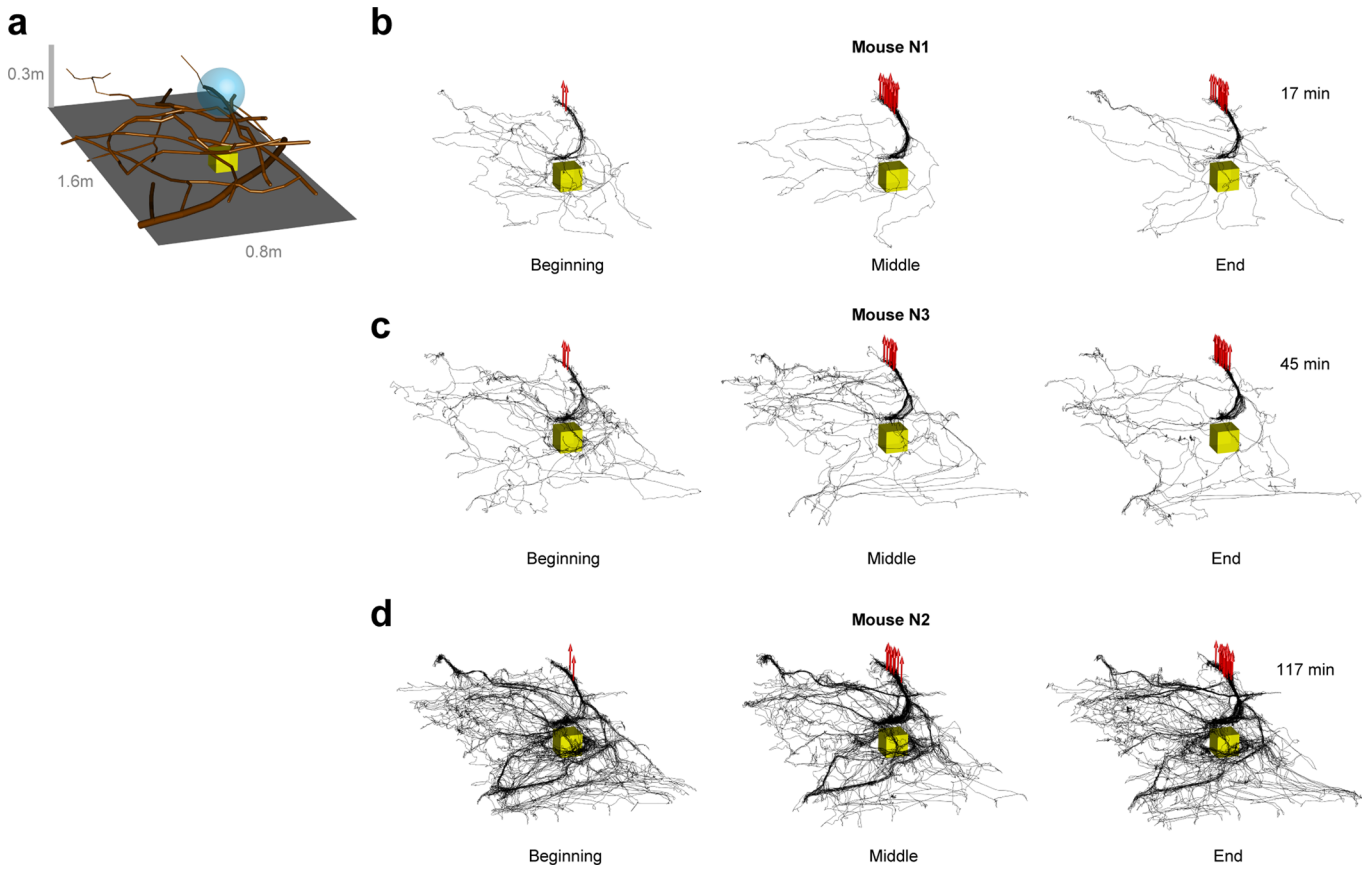

Extended Data Fig. 5 | Mouse operant-conditioning of automatically detected behavior in naturalistic environments. a–c, Additional 3D trajectories of three mice during conditioning of automatically detected postures. The time to reach the criteria condition (50th rearing) is noted on the right.

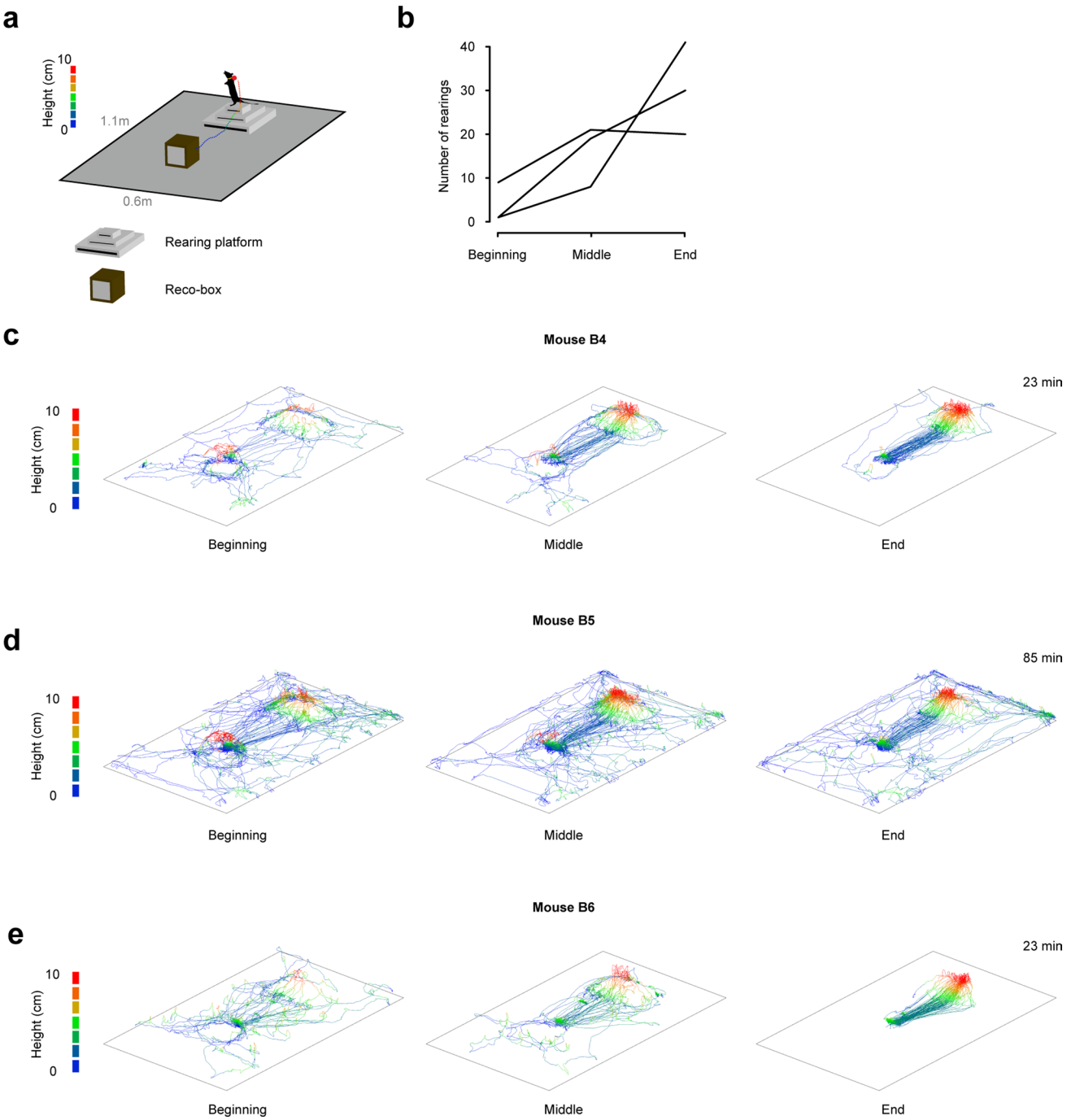

Extended Data Fig. 6 | Mouse operant-conditioning of automatically detected behavior in an open-field arena. a, Open-field arena for mice with an elevated platform and a RECO-box. The color code indicates the height of the tracked marker on the neck of the mouse. **b**, Summary data from 3 mice across the sessions (N=3 mice). **c**–**e**, Trajectories of three mice during condition sessions where the number of rearings increased. The time to reach the criteria condition (50th rearing) is noted on the right.

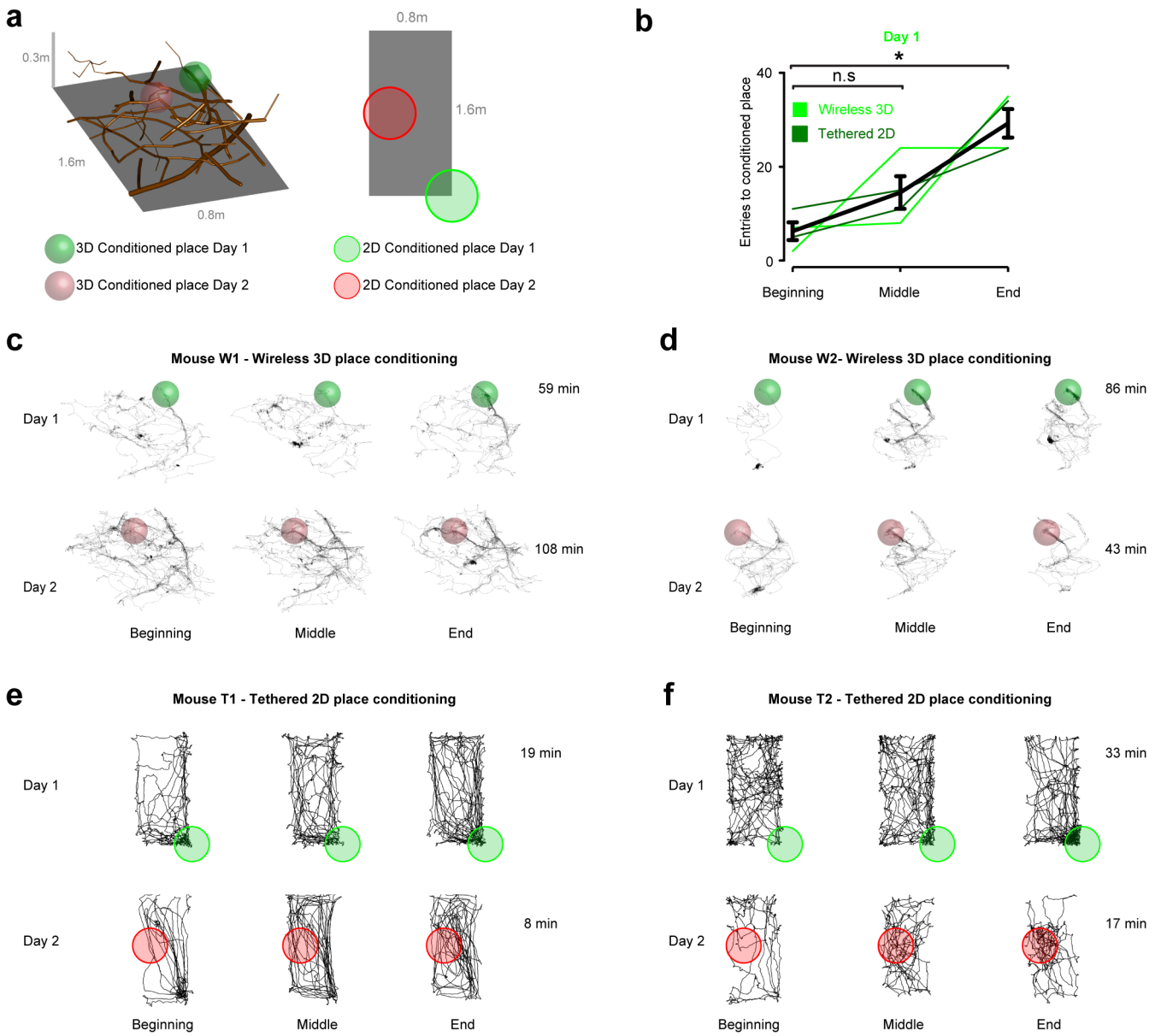

Extended Data Fig. 7 | Place-conditioning using wireless and tethered optogenetic stimulation of VTA. a, The red and green spheres indicate the conditioning locations in a naturalistic arena for mice using wireless optogenetics. **b**, Summary data of first day place conditioning session using wireless (3D, 2 mice) and tethered (2D, 2 mice) optogenetic VTA stimulation. The data from the wireless and tethered optogenetic were grouped together based on the day the place conditioning experiments were carried out. Mice were naive on the first day. The number of entries to the conditioned place increased within a session (N= 4 mice; one-way repeated measure ANOVA; F(2,6)=10.916; main effect P=0.01; pairwise two-sample t test; Bonferroni correction for multiple comparison; beginning versus end *P=0.025; beginning versus middle; P=053; n.s is not significant). Error bars represent SEM. **c**,**d**, Original trajectories of two place-conditioning sessions in 3D environment using wireless optogenetics for two mice (trajectories for Day 2 in (**d**) are the same as the one shown in Fig 5.**c**, The colored spheres (red and green) show the conditioned places. **e**,**f**, Original trajectories of two place conditioning sessions for two mice in the open-field arena using tethered optogenetics. The colored circles (red and green) show the conditioned locations. The time to reach the criteria condition (50th entrance to the conditioned place) is noted on the right.

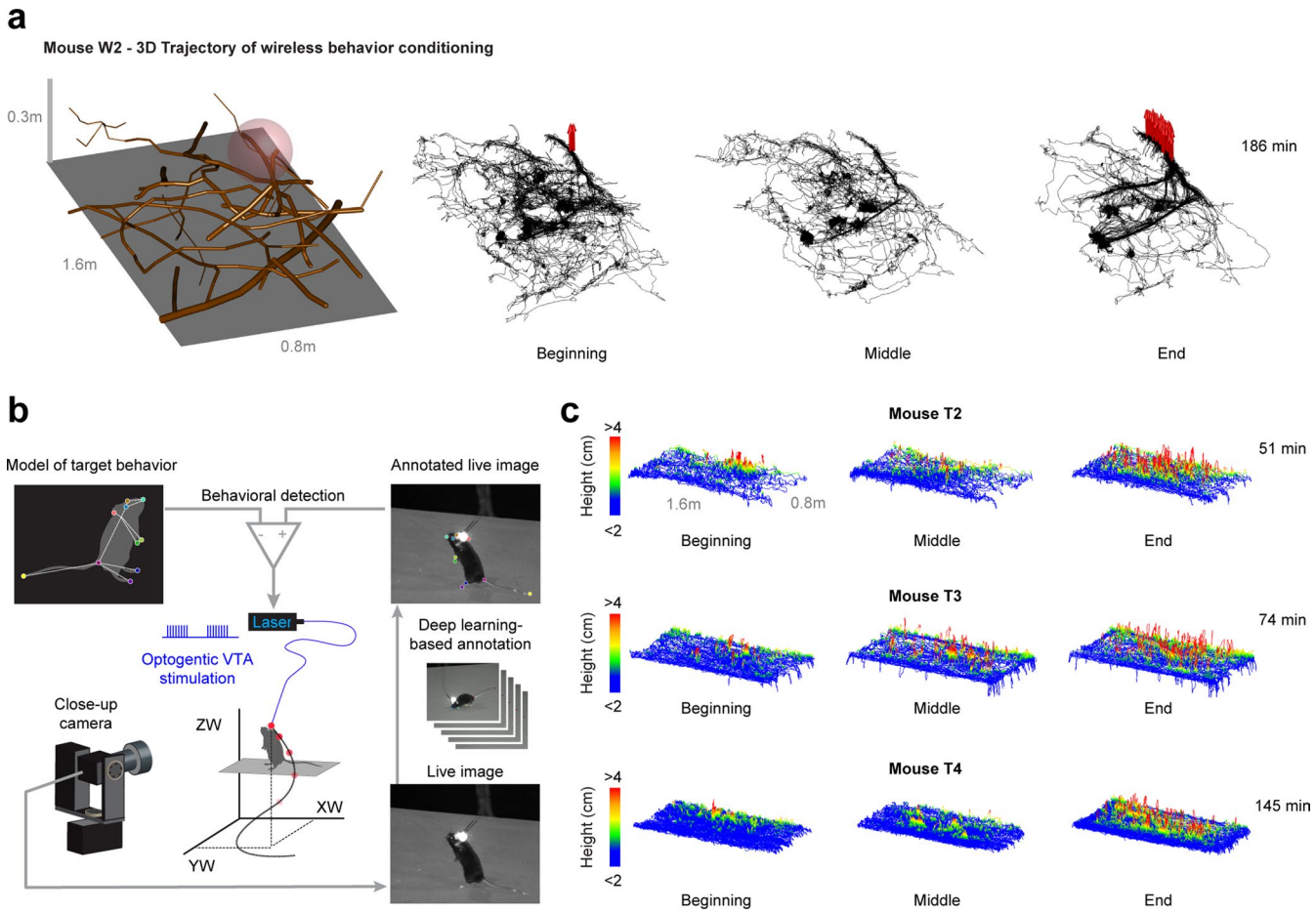

Extended Data Fig. 8 | Automatically reinforcing postures using wireless and tethered optogenetic VTA stimulation. a, A arena covered with branches for mice with an experimenter-defined area where rearing was conditioned (red sphere). 3D trajectories of an additional mouse during a session with optogenetic reinforcement of an automatically detected behavior syllable (rearing, red arrows). **b**, Schematic representation of the information flow during optogenetic VTA DA neurons stimulation in 2D open-field arena. The steps are identical to Fig. 6a, except that the detection of a behavioral event triggers tethered optogenetic stimulation of VTA DA neurons. **c**, 3D trajectory of three mice during the session of reinforcement of an automatically detected behavior syllable (rearing) using tethered optogenetics in 2D environment. The color code indicates the height of the mouse. The time to reach the criteria condition (100th rearing) is noted on the right.

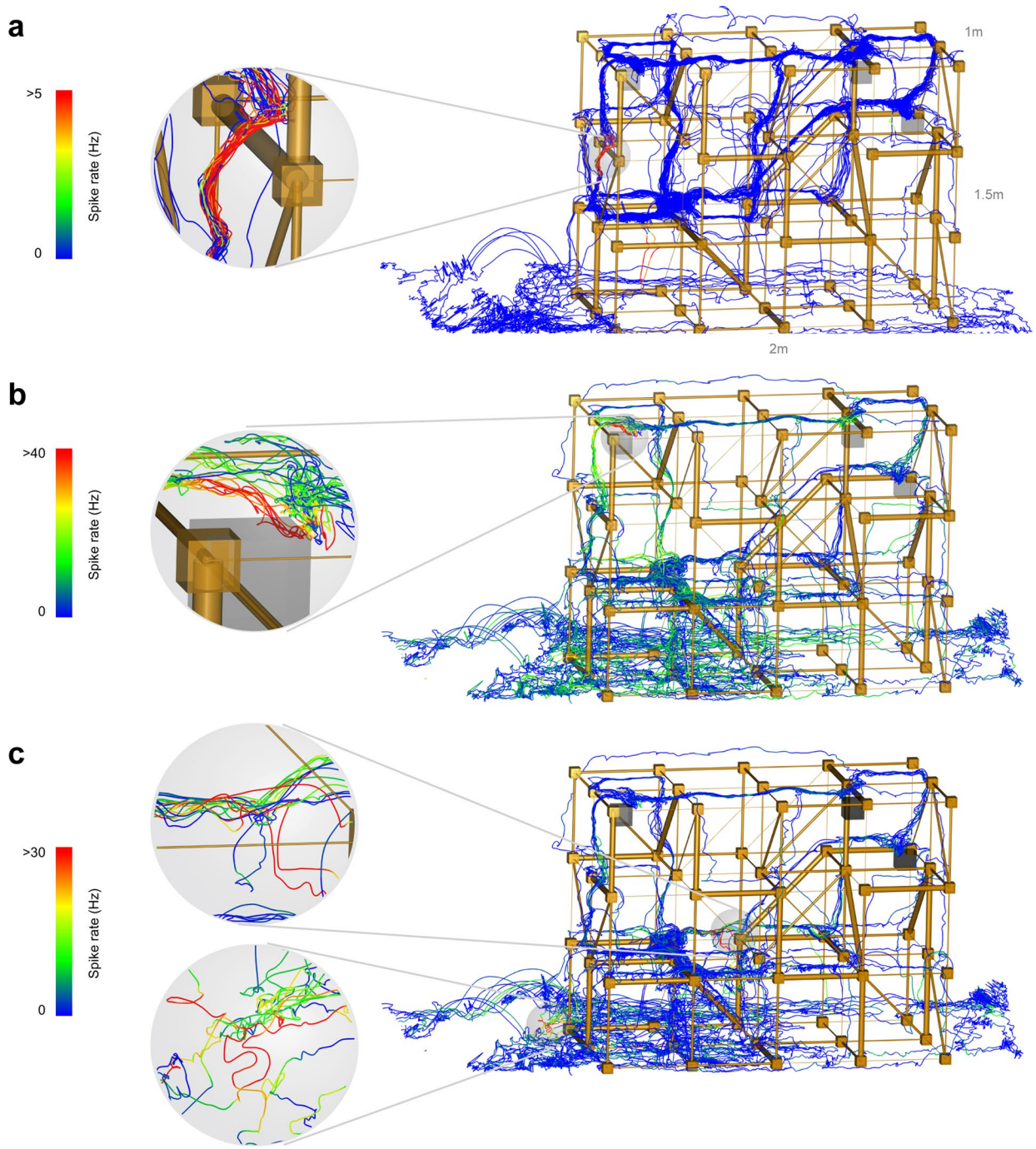

Extended Data Fig. 9 | Additional CA1 neurons with spatially restricted activity. a, CA1 neuron showing increased activity preferentially on a single branch. **b**, CA1 neuron from different session (but same animal) showing increased activity near a feeder (gray square). **c**, CA1 neuron from the same session as (**b**) but showing increased activity at two different locations.

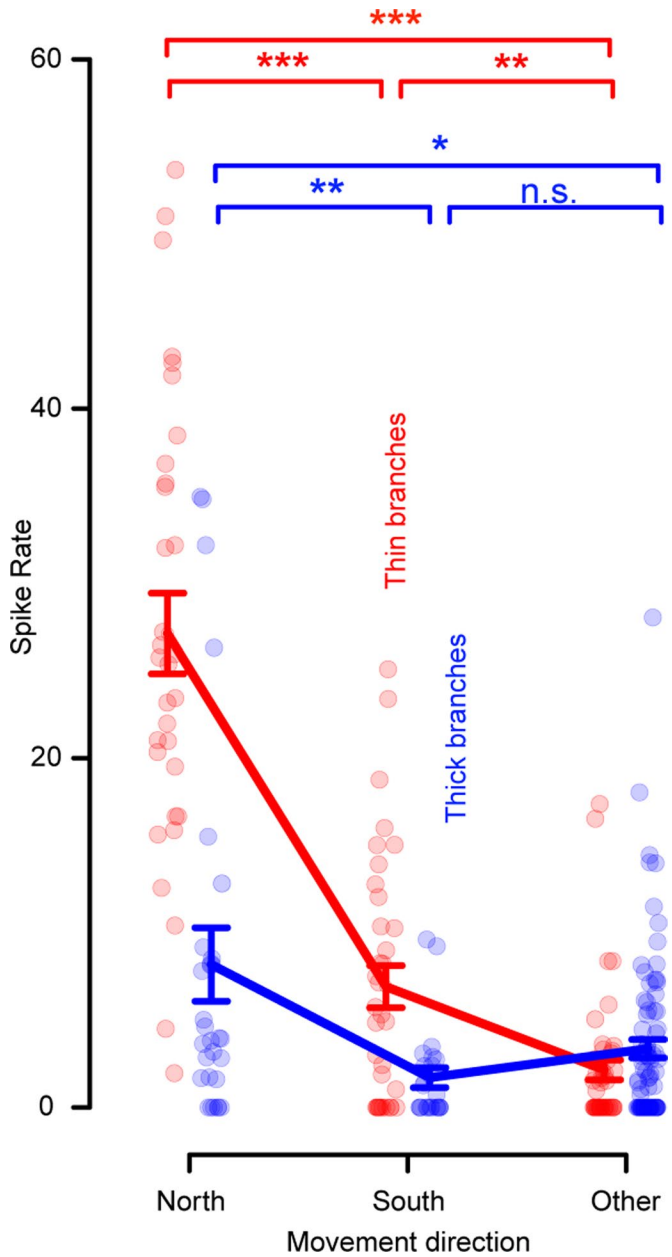

Extended Data Fig. 10 | Detailed analysis of a directional cell (Fig. 6). This neuron showed the highest activity when moving on a thin branch towards the north of the maze. Each dot represents the average spike rate during a 13cm segment. Kruskal-Wallis tests; main effect *P*=1.110-14for thin (red) and P=0.007 for thick (blue) branches; Wilcoxon rank sum test for multiple comparison; Holm adjustment; red; N=32, N=35 and N=46 for North, South and Rest; North versus South; ***$P < 10^{-8}$; North versus Rest; ***$P < 10^{-8}$; South versus Rest; **P=0.0018; blue; N=27, N=23 and N=84 for North, South and Rest; North versus South; **P=0.006; North versus Rest; *P=0.03; South versus Rest; P=0.14; n.s not significant;). Bars represent the standard error of mean.

nature research

Corresponding author(s): Daniel Huber

Last updated by author(s): Jul 13, 2020

Reporting Summary

Nature Research wishes to improve the reproducibility of the work that we publish. This form provides structure for consistency and transparency in reporting. For further information on Nature Research policies, see Authors & Referees and the Editorial Policy Checklist.

Statistics

For all statistical analyses, confirm that the following items are present in the figure legend, table legend, main text, or Methods section.

n/a	Confirmed	
☐	☒	The exact sample size (*n*) for each experimental group/condition, given as a discrete number and unit of measurement
☐	☒	A statement on whether measurements were taken from distinct samples or whether the same sample was measured repeatedly
☐	☒	The statistical test(s) used AND whether they are one- or two-sided *Only common tests should be described solely by name; describe more complex techniques in the Methods section.*
☒	☐	A description of all covariates tested
☐	☒	A description of any assumptions or corrections, such as tests of normality and adjustment for multiple comparisons
☐	☒	A full description of the statistical parameters including central tendency (e.g. means) or other basic estimates (e.g. regression coefficient) AND variation (e.g. standard deviation) or associated estimates of uncertainty (e.g. confidence intervals)
☐	☒	For null hypothesis testing, the test statistic (e.g. *F*, *t*, *r*) with confidence intervals, effect sizes, degrees of freedom and *P* value noted *Give P values as exact values whenever suitable.*
☒	☐	For Bayesian analysis, information on the choice of priors and Markov chain Monte Carlo settings
☒	☐	For hierarchical and complex designs, identification of the appropriate level for tests and full reporting of outcomes
☒	☐	Estimates of effect sizes (e.g. Cohen's *d*, Pearson's *r*), indicating how they were calculated

Our web collection on statistics for biologists contains articles on many of the points above.

Software and code

Policy information about availability of computer code

Data collection	Custom C &C++ (gcc 5.4.0) code (using OpenCV 3.1) was used for animal tracking and all the closed-loop control. Real-time visualization of 3D trajectories was done using gnuplot (5.2) .Real-time behavior analysis was done using a custom programmed (Python 3) real-time version of DeepLabCut (1.0) software (Mathis et al. 2018). Electrophysiology recordings was acquired using Trodes software (1.8.1, SpikeGadgets). Custom Arduino (1.8.5) code was used to program the RECO-boxes.
Data analysis	All the analysis of tracking data, statistics and plots were done using R (3.4.4) software. Spike sorting was done using SpykingCircus (only one version exists). Analysis of tetrode position in the mouse lemur brain was done using Amira software (6.0.0).

For manuscripts utilizing custom algorithms or software that are central to the research but not yet described in published literature, software must be made available to editors/reviewers. We strongly encourage code deposition in a community repository (e.g. GitHub). See the Nature Research guidelines for submitting code & software for further information.

Data

Policy information about availability of data

All manuscripts must include a data availability statement. This statement should provide the following information, where applicable:

- Accession codes, unique identifiers, or web links for publicly available datasets
- A list of figures that have associated raw data
- A description of any restrictions on data availability

All figure data is provided in the Supplementary Data section. The original raw data (videos, electrophysiological recordings, 3D trajectories) is available upon request. The MRI Atlas for mouse lemur is available at: https://www.nitrc.org/projects/mouselemuratlas.

Field-specific reporting

Please select the one below that is the best fit for your research. If you are not sure, read the appropriate sections before making your selection.

☒ Life sciences ☐ Behavioural & social sciences ☐ Ecological, evolutionary & environmental sciences

For a reference copy of the document with all sections, see nature.com/documents/nr-reporting-summary-flat.pdf

Life sciences study design

All studies must disclose on these points even when the disclosure is negative.

Sample size	Sample size was not predetermined in this study for both mice and mouse lemurs. We used 4 mice in 3D arena and 6 mice for open-field arena for closed-loop experiments and 5 mice for optogenetics experiments to be able to perform statistical analysis on their performance. For the mouse lemur closed-loop experiments we only used one mouse lemur as a proof of principle that our system can produce same results with primates. For the social behavior analysis of mouse lemurs we used 3 mouse lemurs (2 male and 1 female) and run experiments with male-male and female-male mouse lemurs to be able to compare their social interaction. For the electrophisiology experiments we only recorded neuronal activity from two mouse lemurs.
Data exclusions	We did not exclude any data.
Replication	We repeated experiments with multiple mice for place conditioning (N=4 for 3D arena, N=6 for 2D arena), behavior conditioning (N=4 for 3D arena, N=3 for open field), operant conditioning via wireless optogenetic stimulation (N=2) and tethered optogenetic stimulation (N=2 for place conditioning and N=3 for behavior conditioning) to demonstrate system's ability to reproduce the same data in different experimental conditions (multiple conditioned locations in both the 3D and open-field arena). The replication was successful as reported in Extended Data Figures 2-8 in addition to Figures 3-5. Additionally we performed the same conditioning experiments for one mouse lemur (2 different location for place conditioning and rearing for behavior conditioning) as a proof of principle that we can reproduce the same data with primates. The replication for place conditioning experiment in mouse lemur was successful as reported in Extended Data Fig 4.
Randomization	We did not divide animals into different experimental groups.
Blinding	We did not perform any blinding since all the data acquisition and the pipeline for the analysis was automatically done.

Reporting for specific materials, systems and methods

We require information from authors about some types of materials, experimental systems and methods used in many studies. Here, indicate whether each material, system or method listed is relevant to your study. If you are not sure if a list item applies to your research, read the appropriate section before selecting a response.

Materials & experimental systems

n/a	Involved in the study
☐	☒ Antibodies
☒	☐ Eukaryotic cell lines
☒	☐ Palaeontology
☐	☒ Animals and other organisms
☒	☐ Human research participants
☒	☐ Clinical data

Methods

n/a	Involved in the study
☒	☐ ChIP-seq
☒	☐ Flow cytometry
☒	☐ MRI-based neuroimaging

Antibodies

Antibodies used	In this study, the following primary antibodies was used: rabbit polyclonal anti-Tyrosine Hydroxylase (1/500 dilution, abcam, ab6211). The following secondary antibodies was used: donkey polyclonal anti-rabbit 555 (Alexa Fluor - 1/500 dilution, abcam-ab150062).
Validation	The antibodies used in the study were commercially available antibodies validated for IHC and WB experiments in rodents. For references of the primary antibody: https://www.abcam.com/tyrosine-hydroxylase-antibody-ab6211.html and the secondary antibody:https://www.abcam.com/donkey-rabbit-igg-hl-alexa-fluor-555-preadsorbed-ab150062.html under the References section.

Animals and other organisms

Policy information about studies involving animals; ARRIVE guidelines recommended for reporting animal research

Laboratory animals	Mice used for all experiments in 3D arena were adult C57Bl/6J (N=4 mice; 2 males and 2 females; mice were 18, 18, 12 and 12

Laboratory animals	weeks old during the experiment). Mice used in the operant conditioning using optogenetic stimulation were adult DAT-iresCre mice (Slc6a3tm1.1(cre)Bkmn/J; tethered optogenetics; N=3 mice; 2 females and 1 male; mice were 13,13 and 48 weeks old during experiment; wireless optogenetics; N=2 mice; both female; mice were 17 and 27 weeks old during experiment). Mice used for experiments in open-field arena were adult C57Bl/6J (N=6 mice; 5 females and 1 male; mice were 29, 34, 34, 11, 11 and 26 weeks old during experiment). 4 adult grey mouse lemurs (Microcebus murinus) were used for this study. All mouse lemurs were born and raised in the “Mouse Lemur Platform” of the Museum of Natural History in Brunoy, France (N=4 mouse lemurs; 3 males and 1 female; mouse lemurs were 1.5, 3, 2.5 and 3 years old during experiment).
Wild animals	No wild animals were used for this study.
Field-collected samples	No field-collected samples were used for this study.
Ethics oversight	The procedures with mouse lemurs are in accordance with European animal welfare regulations and were reviewed by the local ethics committee (“Comité d’éthique en expérimentation animale No. 68”) in Brunoy, France, by the ethics committee of the University of Geneva, Switzerland, and authorized by the French “Ministère de l'éducation nationale de l'enseignement supérieur et de la recherche”. All experiments with mice were carried out in Geneva, Switzerland, and reviewed by the local ethics committee and authorities of the Geneva canton ("Institutional Animal Care and Use Committee of the University of Geneva and Geneva veterinary offices.").

Note that full information on the approval of the study protocol must also be provided in the manuscript.